AUTOMATED DETECTION AND DIAGNOSIS OF BRAIN TUMORS USING MRI IMAGES

CONTENTS

CHAPTER PAGE-NO

SYNOPSIS

Brain Tumor is either a cancerous or a non-cancerous mass of abnormal cells in the brain. In this work, we have considered three types of brain tumors. They are meningioma tumor, glioma tumor and pituitary tumor. Meningioma is a tumor that develops in the membranes that surround the brain and spinal cord, known as the meninges. Glioma is a brain tumor that affects the brain and spinal cord. Gliomas start in the gluey supporting cells (glial cells) that surround and help nerve cells operate. Pituitary tumors are abnormal growths in the pituitary gland that develop over time.

To increases the survival rate of the brain tumor patients and to have an improved treatment technique in medical image processing, brain tumor segmentation is essential method of diagnosis. For brain tumor detection and diagnosis, the brain tumor segmentation can be done manually from MRI, which gives the poor level of accuracy and identification. The classification of abnormalities is not only predictable and straightforward, but also is a time-consuming task for physician. Nowadays, the issue of automatic segmentation and analysis of brain tumors are major research area. However, the detection of tumor is a challenging task since tumor possesses complex characteristics in appearance and boundaries. Diagnosis of a brain tumor is visualised to a doctor in the form of a report. Hence, we are building a system which automates the process of generating a preliminary report for detection and diagnosis of brain tumor.

This project work presents an automated detection and diagnosis of brain tumor using MRI Images, where we build a system which automatically generates a preliminary report which contains the type of tumor, its corresponding ICD code, tumor diameter and tumor area along with the original input image with the tumor highlighted for visualization. This will be achieved through classification and segmentation of the MRI Images, where the classification will be done to identify the tumor type and ICD code and segmentation will be done to visualize the tumor and to find its diameter and area. For our project, a preliminary report is being constructed which utilizes one MRI image of a brain tumor to diagnose tumor diameter and tumor area.

CHAPTER 1
INTRODUCTION

In all vertebrate and most invertebrate organisms, the brain functions as the nerve system's. It's found in the head, usually near the vision-controlling sensory organs. It is the most complex organ in a vertebrate's body. In a human, the cerebral cortex contains 14–16 billion neurons[1].

The average brain weighs 350-400 grammes at birth, accounting for around 25% of the ultimate adult brain weight of 1.4-1.445 kg and just 2% of whole-body mass, which is attained between 10 and 15 years of age [3]. The fastest increase happens during the first three years of life, with about 90% of adult value reaching by the age of five. Its usual width is around 140 mm, length is around 167 mm, and height is around 93 mm. While the brain changes throughout our lives, changes in brain morphology during childhood, adolescence, and adulthood are far more subtle than those in the first four years [4].

The cerebrum (outer layer is the cerebral cortex), the cerebellum, and the brain stem at the base of the brain are the three primary structural divisions of the brain (which extends from the upper cervical spinal cord to the diencephalon of the cerebrum)[5].

The cerebrum is the biggest structure in the brain. The surface of the cerebrum is made up of depressions or grooves (sulci) and ridges or raised areas (gyri), which increase the surface area of the cerebrum without increasing the brain's size. The cerebrum's outer surface is made up of grey matter, which is about 2 to 4 mm thick and processes and integrates information from white matter fibre tracts on the inner surface[6] hemispheres, the right and left, which are connected by the corpus callosum, which facilitates communication between both sides of the brain. Each hemisphere receives information from the contralateral side of the body, resulting in motor control of the right side of the body and vice versa. After then, the Hemispheres are separated into four lobes.

The cerebellum is placed in the posterior cerebral fossa, inferior to the tentorium cerebella or tentorial membrane and posterior to the fourth ventricle, pons, and medulla oblongata. The cerebellum is just around 10% of the total size of the brain, yet it includes more than half of the total number of neurones[6]. The cerebellum is largely engaged in movement coordination and learning (motor learning), and it has ipsilateral movement control, which means that the cerebellum's left hemisphere controls the left side of the body and vice versa. It helps to maintain balance and posture by controlling the initiation, timing, sequencing, and force generation of muscular contractions, as well as the order of muscle firing when a group of muscles works together to produce a movement[6].

The brainstem, which begins at the foramen magnum and extends to the posterior cranial fossa of the skull, is the oldest section of the brain. The medulla oblongata, pons, and midbrain are the three regions. It connects the forebrain to the spinal cord's narrowing [6].

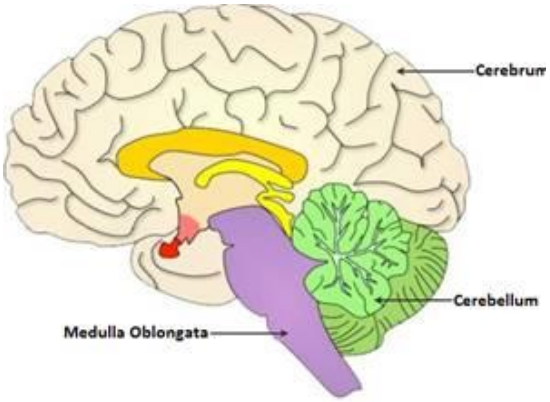

Fig 1.1 Human Brain [2]

1.1 BRAIN TUMOR

A brain tumour is a development of aberrant brain cells that can be malignant or non-cancerous. New or worsening headaches, impaired vision, loss of balance, disorientation, and seizures are all indications of a brain tumour. In certain circumstances, there may be no symptoms. Tumors can occur in the brain, or cancer from other parts of the body can travel to the brain. Surgery, radiation, and chemotherapy are all choices for treatment[7]. 85–90 % of all primary central nervous system (CNS) tumours are brain tumours. In 2020, an estimated 308,102 people will be diagnosed with a primary brain or spinal cord tumour worldwide. This year, approximately 4,170 children under the age of 15 will be diagnosed with a brain or CNS tumour in the United States [8]. The three more common types of brain tumor which we have detected and diagnosed in our project is shown below:

1.1.1 MENINGIOMA

Meningioma is a tumour that develops in the membranes that surround the brain and spinal cord, known as the meninges. It is classified as a brain tumour even though it is not strictly a brain tumour because it has the potential to compress or press on nearby brain, nerves, and arteries. The most frequent type of tumour that arises in the head is meningioma. The vast majority of meningiomas grow slowly and often go unnoticed for years. On the other hand, their impact on neighbouring brain tissue, nerves, or arteries can sometimes result in significant disability. Meningiomas are more frequent in women and are diagnosed later in life, but they can strike at any age [9]. Most meningiomas do not require immediate treatment since they grow slowly and frequently without generating any symptoms.

1.1.2 GLIOMA

Glioma is a form of brain tumour that can damage the brain as well as the spinal cord. Gliomas start in the gluey supporting cells (glial cells) that surround nerve cells and help them operate. Glial cells can become tumours in three ways.

Gliomas are categorised based on the type of glial cell that is involved in the tumour, as well as the tumor's genetic traits, which can help predict how the tumour will behave over time and which treatments will be most effective. A glioma can impede brain function and be fatal depending on its location and rate of growth. Gliomas are an extremely prevalent kind of primary brain tumour [10]. The type of glioma a patient has has an impact on therapy and prognosis. Glioma treatment options include surgery, radiation therapy, chemotherapy, targeted therapy, and experimental clinical trials [10].

1.1.3 PITUITARY TUMOR

Pituitary tumours are malignant growths in the pituitary gland that develop over time. Some pituitary tumours overproduce hormones that control important physiological functions. The pituitary gland may produce less hormones as a result of some pituitary tumours. Pituitary tumours are almost always benign (noncancerous) growths (adenomas). Adenomas are benign tumors that do not spread outside of the pituitary gland or surrounding organs. Surgical removal, growth control, and hormone level pharmaceutical therapy are among options for treating pituitary tumors. Observation is possible [11]. Figure 1.2 shows the MRI image of the three different brain tumor.

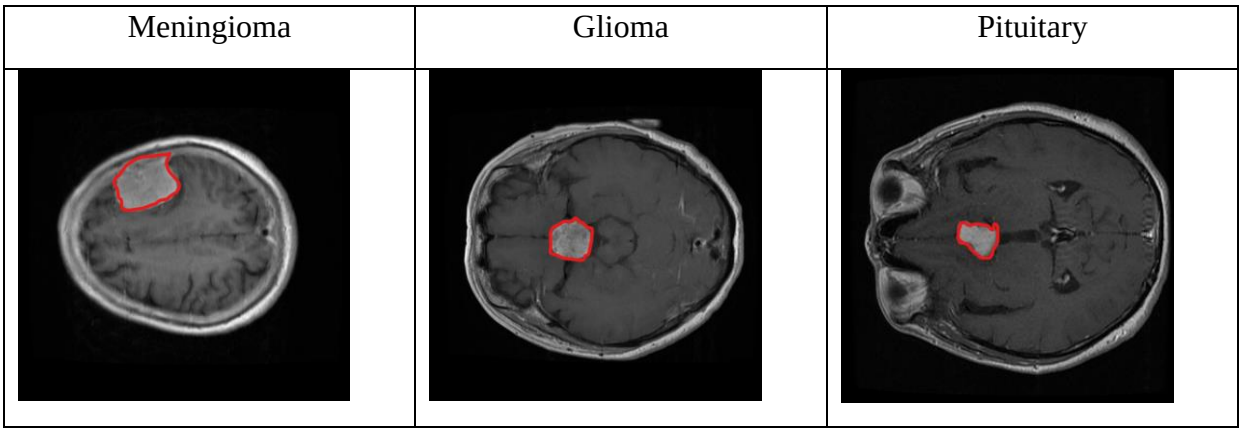

Fig 1.2 MRI image of the brain tumors.

1.2 BRAIN TUMOR DIAGNOSIS

To locate and diagnose a brain tumour, as well as to determine the type of tumour, doctors use a variety of tests. They also run tests to detect if the cancer has spread to other places of the body since it first appeared. This is referred to as metastasis, and it is unusual in primary brain tumours. Doctors may also conduct tests to discover the most effective therapies. For most forms of tumours, taking a sample of the possible tumour is the only sure way for a clinician to know if an area of the body contains a tumour [12]. A biopsy or surgical removal of some or all of the tumours can accomplish this. A biopsy is when a doctor extracts a small sample of tissue for laboratory testing. If this is not possible, the doctor may recommend other tests to aid in the diagnosis. Doctors can use imaging studies to determine if the tumour is a primary brain tumour or cancer that has spread to the brain from elsewhere in the body. Images of the inside of the body are produced via imaging tests [12].

When choosing a diagnostic test, doctors may take into account the type of tumour suspected, signs and symptoms, age and general health, the findings of previous medical tests, and so on. In general, magnetic resonance imaging is used to diagnose a brain tumour (MRI). When an MRI reveals a brain tumour, the most frequent technique to diagnose the type of tumour is to examine the results of a biopsy or surgery on a sample of tissue. A preliminary report is being created for our project that uses one MRI scan of a brain tumor to determine tumor diameter and tumor area

1.2.1 TUMOR TYPE

When cells replicate too quickly, a tumour forms. Tumors can range in size from a little nodule to a massive mass, and they can appear practically anywhere on the body, depending on the type. The type of tumour is a crucial diagnostic factor. For our project, we are going to focus on detection and diagnosis of the three types of brain tumor: meningioma, glioma and pituitary.

1.2.2 ICD CODE

The International Classification of Diseases (ICD) is a system for collecting, processing, classifying, and presenting mortality information that promotes international comparability. The classification structure and selection and modification methods included in the applicable revision of the ICD, issued by the World Health Organization (WHO), are then used to convert the reported conditions into medical codes. By giving preference to particular categories, unifying conditions, and systematically picking a single cause of death from a reported sequence of conditions, these coding procedures improve the utility of mortality statistics [13]. In our generation of our preliminary report, we include the corresponding ICD code for the type of tumor diagnosed. For meningioma tumor, the corresponding ICD code is D32.9, For glioma tumor, the corresponding ICD code is C71.9, and for pituitary tumor, the corresponding ICD code is E23.7.

1.2.3 TUMOR DIAMETER

On pathologic evaluation, tumor diameter is defined as the maximum size of the invasive component of the primary tumor [14]. Many staging methods include a clinical assessment of tumor size as an independent predictor of survival [14].

1.2.4 TUMOR AREA

The tumor area is defined as (tumor length) × (maximum tumor depth) [14]. Tumor area can give us an in-depth analysis for clinical evaluation.

1.3 THE NEED FOR AUTOMATION OF BRAIN TUMOR DIAGNOSIS

Brain tumour segmentation is an important method of diagnosis for improving brain tumour patients' survival rates and developing a better treatment procedure in medical image processing. Manual brain tumour segmentation using an MRI for detection and diagnosis is possible, but it has a low level of accuracy and identification. The classification of abnormalities is not only unpredictable and difficult for doctors, but it is also time consuming. Nowadays, automatic segmentation and analysis of brain tumours is a hot research topic. Tumor detection, on the other hand, is a difficult task due to the complexity of tumour appearance and boundary features [15].

1.4 OBJECTIVES OF THE PROJECT

This project presents an automated detection and diagnosis of brain tumor using MRI images, where we build a system which automatically generates a preliminary report which contains the type of tumor, its corresponding ICD code, tumor diameter and tumor area along with the original input image with the tumor highlighted for visualization. This will be achieved through classification and segmentation of the MRI images, where the classification will be done to identify the tumor type and ICD code and segmentation will be done to visualize the tumor and to find its size and area. For our project, a preliminary report is being constructed which utilizes one MRI image of a brain tumor to diagnose tumor diameter and tumor area.

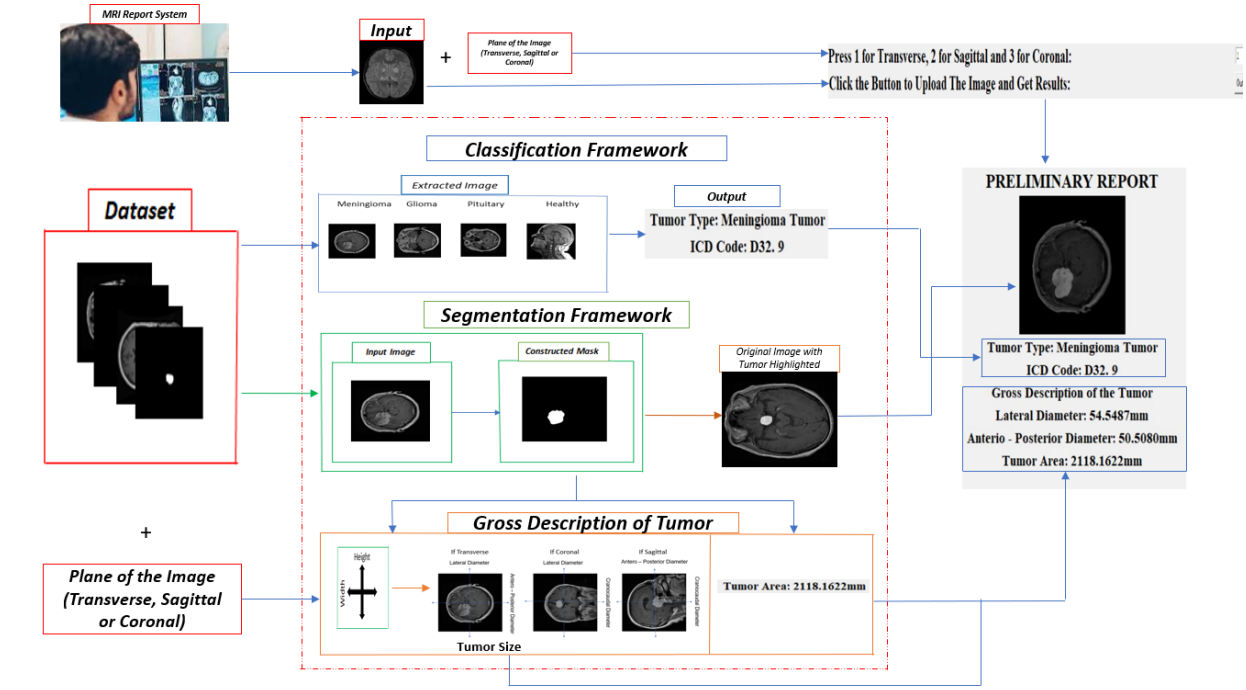

Fig 1.1 Report Generation Framework

CHAPTER 2
LITERATURE SURVEY

This chapter presents the literature survey on Automated Detection and Diagnosis of Brain Tumor using MRI Images. Literature survey includes of all types of published literature. This survey consists of all existing literatures related to the proposed work.

Meiyan Huang et al., (2014) [16] created a content-based image retrieval (CBIR) system for retrieving T1-weighted contrast-enhanced magnetic resonance imaging (CE-MR) pictures of brain malignancies. When a tumor region is entered as a query into the CBIR system, the system looks for tumors in the same pathological category. The system uses the bag-of-visual-words (BoVW) model with partition learning to extract informative features for representing image contents. In addition, the Rank Error-based Metric Learning (REML) distance metric learning algorithm is presented to bridge the semantic gap between low-level visual data and high-level semantic concepts. The suggested method is tested on a brain T1-weighted CE-MR dataset with three different types of brain cancers (i.e., meningioma, glioma, and pituitary tumor).When compared to the spatial pyramid BoVW approach, the mean average precision (mAP) of retrieval increases beyond 4.6 percent when using the BoVW model with partition learning. In terms of mAP, the distance metric taught by REML surpasses three other known distance metric learning methods. Their proposed strategy increases the mAP of the CBIR system to 91.8 percent, and the precision to 93.1 percent when the system returns the top 10 images. These first findings show that the proposed strategy for retrieving brain tumors in T1-weighted CE-MR images is effective and practicable. Using the proposed method, the precision of the system can achieve 91.8 percent, and when the top 10 images are returned, the precision can reach 93.1 percent.

Jun Cheng et al., (2015) [17] their study focuses on the classification of three types of brain tumors in T1-weighted contrast-enhanced MRI (CE-MRI) images (meningioma, glioma, and pituitary tumor). For natural scene classification, spatial pyramid matching (SPM), which divides the image into increasingly fine rectangular subregions and computes histograms of local features from each subregion, produces excellent results. Because of the wide range of tumor shape and size, this method is not relevant to brain tumors. We offer an approach to improve classification performance in this paper. First, instead of using the original tumor region as the ROI, the augmented tumor region via image dilation is used because tumor surrounding tissues can also provide important tumor type clues. Second, the enhanced tumor is divided into increasingly fine ring-shaped subregions. We use the intensity histogram, gray level co-occurrence matrix (GLCM), and bag-of-words (BoW) model to evaluate the efficacy of the suggested method on a large dataset. Using enhanced tumor region as ROI improves accuracies from 71.39 percent to 82.31 percent, 84.75 percent to 78.18 percent, and 88.19 percent to 83.54 percent for intensity histogram, GLCM, and BoW model, respectively, when compared to using tumor region as ROI. Ring-form partition had improved accuracies by up to 87.54 percent, 89.72 percent, and 91.28 percent, in addition to region augmentation.

Zeju Li et al., (2017) [18] proposed a novel automatic three-dimensional (3D) magnetic resonance imaging (MRI) segmentation method for the clinical diagnosis of glioma, the most common and aggressive brain tumor. The method combined a multipath way convolutional neural network (CNN) and fully connected conditional random field (CRF). The influence of varying depths and numbers of neurons in completely linked layers on tumor segmentation was investigated.

The authors Proposed two types of network architectures that were coupled with 3D data. T2flair MRI images of 160 low-grade glioma patients were used to test the approach. The Dice similarity coefficient (DSC) of the approach was 0.85 for the test set of 101 MRI pictures, based on 59 sets of data training and manual segmentation as the ground truth. The work has produced better LGG segmentation outcomes using the proposed methodology than one of the best CNN tumor segmentation approaches currently available. The approach's results outperformed another state-of-the-art CNN algorithm, which achieved a DSC of 0.76 for the same dataset. It was shown that using this strategy to segment low-grade gliomas produced better results.

Mazin Abed Mohammed et al., (2018) [19] used MR images to suggest a new segmentation strategy for brain tissues. Using artificial neural networks, the research presents a fully automatic model-based segmentation and classification strategy for MRI brain tumors. The method uses three computer vision fiction strategies: image enhancement, image segmentation, and non-ROI filtering using texture and HOG features. In order to avoid non-ROI and select the correct object in brain MRI, the filtering out non-ROI process was used in conjunction with histogram analysis. The researchers used 200 MRI instances to compare the automatic and manual segmentation procedures. The fully automatic model-based trainable segmentation outperforms the manual technique and brain identification using ROI texture features, according to the results. With 89 sensitivity and 94 specificity, the reported identification precision is 92.14 percent.

Wei Chen et al., (2019) [20] propose a novel Separable 3D U-Net architecture using separable 3D convolutions. For the characteristics of the isotropic resolution of brain tumor MR images, they design a new separable 3D convolution architecture by dividing each 3D convolution into three branches in a parallel fashion, each with a different orthogonal view, namely axial, sagittal and coronal. proposed a separable 3D block that takes advantage of the state-of-the-art residual inception architecture. Finally, based on separable 3D convolutions, they propose the S3D-UNet architecture using the prevalent U-Net structure. This network has been evaluated on the BraTS 2018 Challenge testing dataset and achieved an average Dice scores of 0. 68946, 0. 83893 and 0. 78347 for the segmentation of enhancing tumor, whole tumor, and tumor core, respectively. However, the high median values show that the testing set may contains some difficult cases, resulting in the lower average scores. In this paper, they have demonstrated that the U-Net with separable 3D convolutions can achieve promising results in the field of medical image segmentation.

Hossom H.Sultan et al., (2019) [21] using two publicly accessible datasets, they proposed a DL model based on a convolutional neural network to categorize different brain tumor kinds. The first divides tumors into categories (meningioma, glioma, and pituitary tumor). The other differentiates between the three forms of glioblastoma (Grade A, B, and C).The first and second datasets, respectively, contain 233 and 73 patients with a total of 3064 and 516 photos on T1 weighted contrast-enhanced images. Starting with the input layer, which retains the pre-processed images and continuing through the convolution layers and their activation functions, the proposed network is made up of sixteen layers (3 convolution, 3 ReLU, normalization and 3 Max Pooling layers). Two dropout layers are also employed to avoid overfitting, followed by a fully connected layer and a SoftMax layer to predict the output, and finally a classification layer to yield the predicted class. Even though the dataset is small (due to the variety of imaging viewpoints), data augmentation assisted in producing better results and thus overcoming this issue. In the dataset considered in this work, their proposed architecture attained accuracy of 96.13 percent.

Ali Mohammad Alqudah et al., (2019) [22] utilized Convolutional Neural Network (CNN), one of the most extensively used deep learning architectures to classify a dataset of 3064 T1 weighted contrast-enhanced brain MR images into three groups for grading (classifying) brain cancers (Glioma, Meningioma, and Pituitary Tumor). The primary goal and purpose for this study are to develop a new CNN architecture for grading (classifying) brain cancers using T1-weighted contrast-enhanced brain MR images. The cropped and uncropped brain tumour photographs are saved in a database, and three folders are formed, one for each kind of glioma, meningioma, and pituitary tumour. In this paper, a new CNN architecture is used. The design has eighteen layers to allow the classifier to accurately grade the brain tumour. The dataset was separated into three subsets: training, validation, and testing, with percentages of 70%, 15%, and 15%, respectively. The suggested approach efficiently evaluated the brain tumour, with accuracy rates of 97.4 percent, 99.0 percent, and 99.2 percent for cropped lesions and 97.5 percent, 97.6 percent, and 98.4 percent for uncropped lesions. Most of the approaches presented in the literature in this study have obtained high recognition rates, with the highest being 97 percent. The design was successful in classifying brain tumours into three classifications with good accuracy and sensitivity in all dataset cases: uncropped, cropped, and segmented.

Muhmmad Irfan Sharif et al., (2019) [23] recommended an active deep learning-based feature selection strategy to segment and recognise brain tumours. The BRATS series (2013, 2015, 2017 and 2018) are used to validate the suggested system in this study. The Pixel Increase along Limit (PIaL) technique is used to improve the visual quality of a tumor-affected image. A novel SbDL method is proposed to construct a saliency map with deep and texture features based on distance points for segmentation. Determine discriminative features from a saliency map, a PSO optimization technique is used. There are two stages to the experiments. First, the SbDL segmentation method is evaluated on the BRATS2017 and BRATS2018 datasets. The BRAST2017 dataset's achieved dice score is 83.73 % for core tumour, 93.7 percent for whole tumour, and 79.94 % for enhanced tumour. The dice score obtained for the BRATS2018 dataset is 88.34 % (core), 91.2% (whole), and 81.84 % (all) (enhanced). On BRATS2013, 2014, 2017, and 2018, the classification strategy is used with an average accuracy of more than 92 percent.

Ammar Mohammed et al., (2019) [24] present an improved deep learning model for brain tumor classification from MRI data in this research. They demonstrated an improved method for categorizing brain tumor types using Residual Networks in this research. For the model design, the proposed method utilized Residual Network (ResNet), a sort of deep learning architecture. ResNet50 architecture was employed, which is a Residual Network variation with 50 layers. ResNet enables the training of extremely deep neural networks by introducing the notion of shortcut connections to bypass one or more layers, hence resolving the issue of degraded accuracy, and vanishing gradient that occurred as models became deeper. Horizontal and vertical flips, rotating, shifting, zooming, ZCA whitening, shearing, and brightness manipulation are some of the data augmentation techniques we used to enhance the dataset size and improve accuracy. The model was trained using a benchmark brain tumor MRI pictures dataset comprising 3064 MRI images and assessed using precision, recall, f1-score, and balanced accuracy as performance metrics. Using the ResNet50 architecture, we were able to obtain image-level accuracy of ".99" and patient-level accuracy of "97."

Milica M. Badža, et al., (2020) [25] introduced a novel CNN architecture for the categorization of three kinds of brain tumours. The primary goal of this study is to use a CNN to classify three tumour kinds from an unbalanced database. The generated network was evaluated on T1-weighted contrast-enhanced magnetic resonance imaging and is simpler than pre-existing pre-trained networks. The network's performance was assessed using four approaches: two 10-fold cross-validation procedures and two databases. The network's adaptation capability was evaluated using one of the 10-fold approaches, subject-wise cross-validation, and the improvement was evaluated using an enhanced picture database. The record-wise cross-validation for the enhanced data set yielded the best result for the 10-fold cross-validation approach, with an accuracy of 96.56 percent. The newly created CNN architecture, with its better generalization potential and fast execution speed, might be employed as an effective decision-support system.

Mahnoor Ali et al., (2020) [26] offers a significant yet simple combinative technique that results in superior and accurate predictions by combining two segmentation networks: a 3D CNN and a U-Net. The goal is to create an automated brain tumor segmentation method that will allow for more efficient and accurate delineation of tumours into intra-tumoral classes than existing methods. On the training dataset obtained from the Brain Tumor Segmentation (BraTS) challenge, the networks are trained individually, with hyperparameters optimised for each model. The training set includes 259 patients with high-grade glioma and 76 patients with low-grade glioma, as well as expertly annotated ground truths. The validation set, on the other hand contains 125 cases of unknown grade. The paper used variable assembling to combine the outputs of the two networks and achieve competitive classification accuracy on the BraTS 2019 validation set. The model reached mean dice scores of 0.750.

Wentao Wu et al., (2020) [27] offers a support vector machine approach based on deep convolutional neural networks (DCNN-F-SVM). This work focuses on a glioma segmentation approach based on deep learning, with the goal of automatically and reliably segmenting the glioma region from a brain MRI using the deep learning algorithm. The proposed segmentation model for brain tumours is separated into three steps. A deep convolutional neural network is trained in the first stage to learn the mapping from picture space to tumour marker space. The predicted labels from the deep convolutional neural network training, as well as the test images, are fed into the integrated support vector machine classifier in the second stage. Train a deep classifier in the third stage, a deep convolutional neural network and an integrated support vector machine are connected in series. In comparison to CNN and SVM employed separately, the suggested DCNN-F-SVM has grown, with the three indicators (DSC, sensitivity, and specificity) being 3.5 %, 2.6 %, and 3.2 % higher for SVM and 1.6 %, 0.9 % and 2.4 % higher for CNN. The proposed model, however, still has flaws, such as a long calculation time.

Mobeen Ur Rehman et al., (2020) [28] presents the BU-Net approach for 2D image segmentation as a contribution to brain tumour segmentation research. In the baseline U-Net design, residual extended skip (RES) and wide context (WC) are used in conjunction with the customised loss function. This study proposes the BU-Net network. BU-Net presents two modules for brain image segmentation that are contained in a U-Net architecture. Two benchmark datasets were used to evaluate the proposed BU-Net model. BraTS2017 and BraTS2018 are the datasets in question. The BraTS 2017 dataset contains images from 285 glioma patients, with 210 of them being HGG cases and the rest being LGG instances. Furthermore, the BraTS 2017 validation dataset contains photos of forty-six patients with undetermined grades. The work incorporated two additional blocks into the existing U-Net architecture: residual extended skip (RES) and wide context (WC).

When compared to the baseline U-Net architecture and other existing efficient segmentation models, BU-Net has shown to be a significant improvement. The BU-Net architecture received dice scores of 0.768, respectively.

Francisco Javier Diaz-Pernas et al., (2021) [29] presented a completely automated brain tumor segmentation and classification model based on a Deep Convolutional Neural Network with a multiscale approach. The goal of this research is to create and evaluate a Deep Learning strategy for brain tumour classification and segmentation using a Multiscale CNN. One distinction between this approach and earlier efforts is that input pictures are analysed at three spatial scales via various processing paths. The suggested neural model can evaluate MRI images comprising three types of tumours: meningioma, glioma, and pituitary tumor, in sagittal, coronal, and axial perspectives, and it does not require input image pre-processing to remove skull or vertebral column components in preparation. This method's performance on a publicly accessible MRI imaging dataset of 3064 slices from 233 patients is compared to previously reported conventional machine learning and deep learning approaches. In comparison, this method achieved a tumor classification accuracy of 0.973.

Motahareh Aghalari et al., (2021) [30] discussed an improved UNet-based designs for automated segmentation of brain tumours from MRI images. They developed the powerful Two-Pathway-Residual blocks for the UNet structure and suggested three models. This paper explains the performance of deep neural networks in brain tumor segmentation task. As inputs, three slices from three different MRI modalities are employed in a modified UNet architecture in the same sequence. First, the dark slices of the MRI picture were removed using a two-step pre-processing procedure. The proposed models were then used to segment the picture of the brain tumour. These models were created by modifying the UNet structure with two-pathway-residual (TPR) blocks. Two-pathway-residual blocks use both local and more global properties at the same time. The presented models have the advantages of lowering computing costs, boosting segmentation speed, and not requiring post-processing. The examination of deep neural networks, particularly UNet, demonstrates their outstanding capacity for segmentation tasks. The suggested models were evaluated on the BRATS'2018 database and produced satisfactory results while having a lower computation cost than the previous techniques. The DCS, sensitivity, and PPV criterion values used for the best-proposed model's segmentation results are 89.76 percent, 89.19 percent, and 90.65 percent, respectively.

Buthayna G. Elshaikh et al., (2021) [31] reliably distinguish brain cancers from other brain components, such as grey and white matter and cerebrospinal fluid (CSF). Using k-means and linear discriminant analysis, this work involves classifying the brain image in axial MRI images into normal brain tissues (white matter, grey matter, and cerebrospinal fluid 'CSF') and malignancy. The researchers used axial, sagittal, and coronal images on fifty brain tumour patients who were chosen at random from a group of two hundred. A typical head coil Philips Intera 1.5 Tesla equipment was used to obtain the brain pictures. All genders are represented in the study, with ages ranging from 18 to 83 years old (56.5 17.2). Six parameters were retrieved from normal and abnormal (tumour) brain MRI images by two experienced radiologists using the 3 x 3 window in this study: signal-to-noise ratio, energy, entropy, standard deviation, coefficient of variation, and variance. The total accuracy of the classification procedure was 94.8 %, and the sensitivity for the tumour was 97.3 %, according to the findings of this study. The categorization accuracy for white matter and grey matter was 95.7 % and 89.7 %, respectively, while the accuracy for CSF was 94.3 %.

Emrah Irmak et al., (2021) [32] aspires to use a convolutional neural network to make multi classifications of brain tumor for early diagnosis. Using publicly available datasets, the goal of this paper is to develop three fully automatic CNN models for multi-classification of brain tumours. The first model is intended to detect brain tumours using MRI images as input. The second model is used to determine the type of brain tumor and the third model is used to predict the grade of the tumor. Choosing the most successful network model for the specific application is one of the challenges in Convolutional neural networks. Grid search optimizer is used in this study to create the model and to optimise the CNN model's hyper-parameters. The first constructed CNN model achieves a high-level accuracy of 99.33% in detecting brain tumours. Furthermore, the classification of brain tumor type into glioma, meningioma, pituitary, normal and metastatic is done with a 92.66% accuracy.

Dillip Ranjan Nayak et al., (2022) [33] their study suggests using min-max normalization to categorize 3260 T1-weighted contrast enhanced brain magnetic resonance images into four categories using a CNN-based dense EfficientNet (glioma, meningioma, pituitary, and no tumor). The constructed network is a modified version of EfficientNet that includes dense and drop-out layers. Boost the contrast of tumor cells, the authors coupled data augmentation with min-max normalization. The dense CNN model has the advantage of being able to accurately categorize a small database of images. As a result, the proposed method achieves outstanding overall results. The suggested model was 99.97% correct during training and 97.78% accurate during testing, according to the experimental results. The newly created EfficientNet CNN architecture can be a beneficial decision-making tool in the research of brain tumor diagnostic tests, thanks to its excellent accuracy and favourable F1 score.

Chetana Srinivas et al., (2022) [34] shows a comparison of the performance of CNN-pretrained VGG-16, ResNet-50 and Inception-v3 models for automatic prediction of tumour cells in the brain using transfer learning. This study compares deep pretrained convolution neural networks based on transfer learning architectures to categorize brain MRI images as benign or malignant tumours spontaneously. Each testing stage includes data pre-processing, data augmentation procedures theorised hyperparameter integral tweaking. When validation accuracy drops while training accuracy grows, the architecture is expected to have overfitting issues. The evaluation results demonstrate that all structures achieve training accuracy of greater than 90 percent, with the greatest validation accuracy of 0.8826. The researchers have observed that VGG-16 delivers better accuracy on the trained and tested dataset, based on the performance study of several pretrained CNN models, such as VGG-16, Inception-v3 and ResNet50. Also, with less loss and validation loss, validation accuracy is significantly closer to the accuracy.

CHAPTER 3

PROPOSED METHEDOLOGY

The proposed methodology is designed for the automated detection and diagnosis of brain tumor using MRI images. The details about the dataset we used in the analysis is discussed in this chapter.

3.1 DATASET

A basic introduction on MRI images and the sequence is given below. Magnetic resonance imaging (MRI) is a medical imaging technique used in radiology to create images of the body's anatomy and physiological processes. MRI scanners generate images of the organs in the body by using strong magnetic fields, magnetic field gradients, and radio waves. MRI is more commonly used to detect brain tumours in our bodies [35]. For this project, we are going to utilize MRI images to detect and diagnose brain tumor.

The magnetization properties of atomic nuclei are used in MRI. To align the protons that are normally randomly oriented within the water nuclei of the tissue being examined, a powerful, uniform external magnetic field is used. This alignment (or magnetization) is then disrupted or perturbed by the introduction of an external Radio Frequency (RF) energy. Through various relaxation processes, the nuclei return to their resting alignment and emit RF energy. The emitted signals are measured after a certain period following the initial RF. The Fourier transformation is used to convert the frequency information in the signal from each location in the imaged plane to corresponding intensity levels, which are then displayed as shades of Gray in a pixel matrix arrangement. Several types of images are produced by varying the sequence of RF pulses applied and collected. The amount of time between successive pulse sequences applied to the same slice is referred to as the repetition time (TR). The time between the delivery of the RF pulse and the reception of the echo signal is referred to as the time to echo (TE) [36].

Tissue can be distinguished by two relaxation times: T1 and T2. T1 (longitudinal relaxation time) is the time constant that governs how quickly excited protons return to equilibrium. It is the time it takes for spinning protons to realign with the external magnetic field. T2 (transverse relaxation time) is the time constant that governs how quickly excited protons reach equilibrium or fall out of phase with one another. It is the time it takes for spinning protons to lose phase coherence among nuclei spinning perpendicular to the main field [37].

The three most common MRI sequences are:

T1 – Weighted : short TE and TR times

T2 – Weighted : longer TE and TR times.

Fluid Attenuated Inversion Recovery (FLAIR) : TE and TR times are exceptionally long

Table 3.1. Most common MRI Sequences and their Approximate TR and TE times

	TR (msec)	**TE (msec)**
T1 – Weighted (Short TR and TE)	500	14
T2 – Weighted (Long TR and TE)	4000	90
FLAIR (Very long TR and TE)	9000	114

These MRI Sequences can also be differentiated based on their brightness level on different tissues of the brain namely White Matter, Cortex, Fat within the bone marrow and Cerebral – Spinal Fluid (CSF). Table 3.2 shows the comparison of T1 – Weighted, T2 – Weighted and FLAIR images.

Table 3.2. Comparison of T1 vs. T2 vs. Flair (Brain)

Tissue	**T1 – Weighted**	**T2 – Weighted**	**FLAIR**
CSF	Dark	Bright	Dark
White Matter	Light	Dark Gray	Dark Gray
Cortex	Gray	Light Gray	Light Gray
Fat (Within the bone marrow)	Bright	Light	Light
Inflammation (Infection, Demy lineation)	Dark	Bright	Bright

Figure 3.1 shows T1 – Weighted, T2 – Weighted and FLAIR images on axial region of the brain. For our project, we would be utilizing T1 – Weighted MRI Images for Detection and Diagnosis of Brain Tumor.

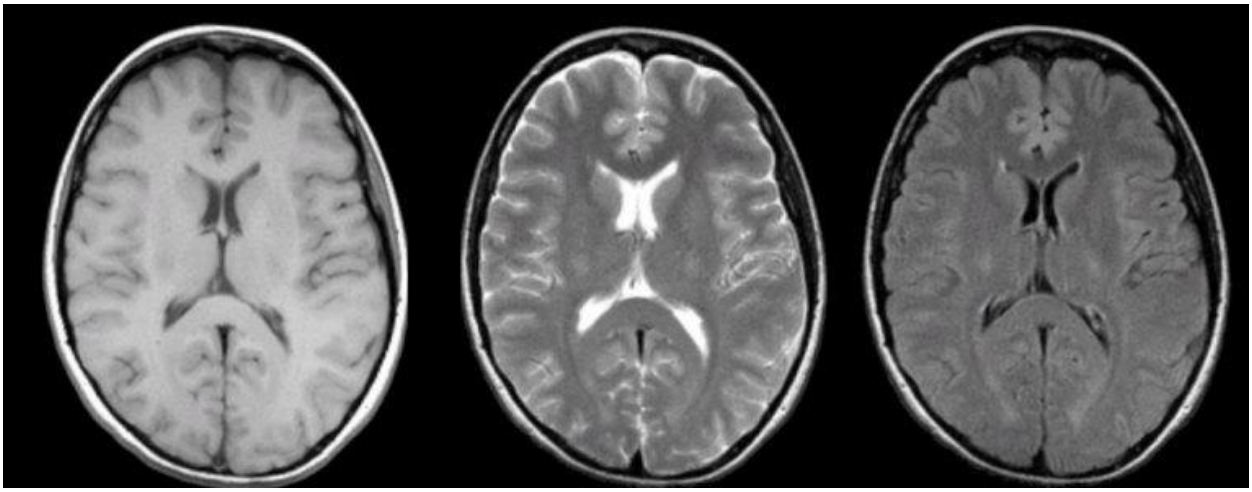

(a) (b) (c)

Fig 3.1. (a) T1 – Weighted, (b) T2 – Weighted, (c) FLAIR (Right)

3.1.1 DATASET DESCRIPTION

Jun Cheng et al., (2015) [37] proposed a brain tumor dataset. It is an open-source dataset which was acquired from Nanfang Hospital, Guangzhou and General Hospital, Tianjin Medical University, China and was taken from the year 2005 to 2010. The dataset was first published online in 2015 and the last modified version was released in 2017. This dataset has been approved by the Ethics Committees of Nanfang Hospital and General Hospital Tianjin Medical University, China. This Dataset was posted by Jun Cheng, School of Biomedical Engineering Southern Medical University, Guangzhou, China

The dataset consists of 3064 slices of T1- weighted contrast enhanced MRI images. All the images were acquired in three planes: Transverse, Sagittal and coronal. Three types of brain tumors namely, Meningioma, Glioma and Pituitary tumors are apparent in the dataset. Each slice is of 512 x 512 pixels and the size of the pixel is 0.49mm x 0.49mm. For each patient, 3 experienced radiologists initially consulted the patient pathology report to obtain the pathology type and then labelled the images. Each radiologist dealt with all images independently. Each Patient are Represented by their Patient ID only in this Dataset.

The Dataset contains Meningioma (708 slices), Glioma (1426 slices), and Pituitary tumor (930 slices).

This data is organized in MATLAB data format (.mat file). Each file stores a struct containing the following fields for an image:

cjdata.label: 1 for meningioma, 2 for glioma, 3 for pituitary tumor
cjdata.PID: patient ID cjdata.image: image data
cjdata.tumorBorder: A vector storing the coordinates of discrete points on tumor border. For example, [x1, y1, x2, y2,...] in which x1, y1 are planar coordinates on tumor border. It was generated by manually delineating the tumor border. So, we can use it to generate binary image of tumor mask.
cjdata.tumorMask: A binary image with 1s indicating tumor region.

Figure 3.2 shows a sample of MR image from the dataset which contains three different types of brain tumor detected along three different planes

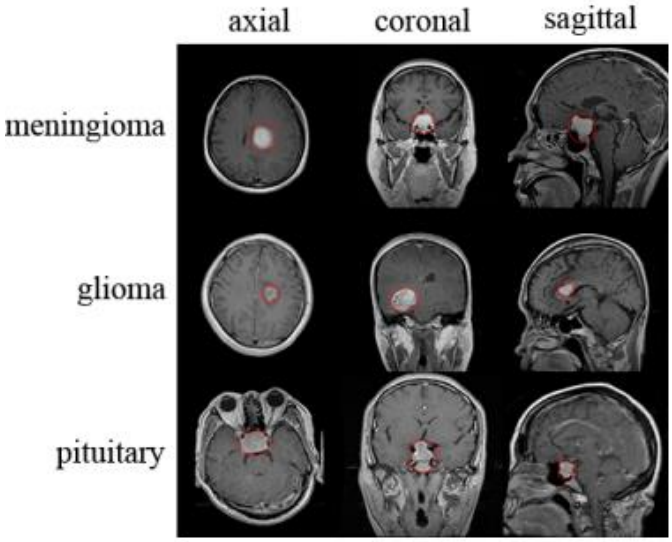

Fig 3.2. MRI Images showing different Brain Tumors in different Planes

For Building a system which automatically generates a preliminary report for detection and diagnosis of brain tumor using a given MRI image, we are adding a healthy control dataset obtained from Kaggle [38]. There are 501 healthy images which are together added with the dataset bringing the total count of MRI images from 3064 images to 3565 images.

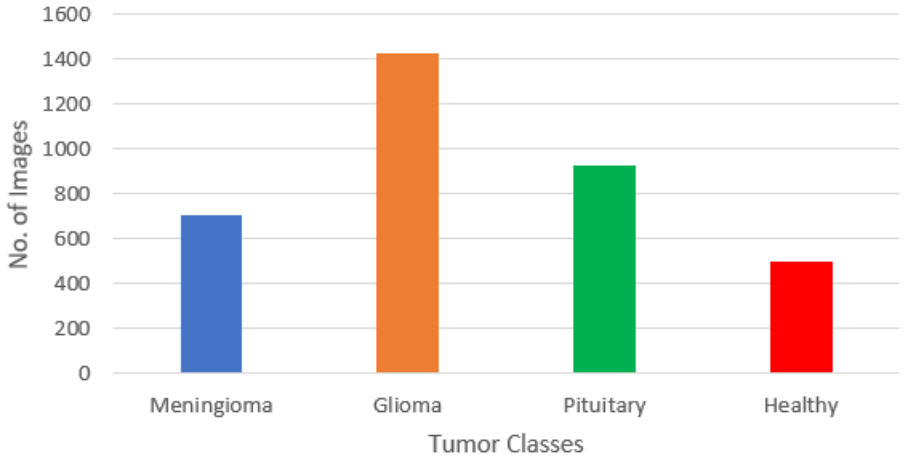

Fig 3.3. No. of Slices present in Each Tumor Class

Table 3.3 and Fig 3.4 shows the number of images present across each classes of tumor along with their planes and the corresponding images present along them.

Table 3.3. No of slices present in each category and views

Tumor Category	No. of Slices	View	No. of Slices
Meningioma	708	Transverse	154
		Sagittal	119
		Coronal	435
Glioma	1426	Transverse	604
		Sagittal	491
		Coronal	331
Pituitary	930	Transverse	236
		Sagittal	416
		Coronal	278
Healthy Control	501	Transverse	357
		Sagittal	97
		Coronal	47

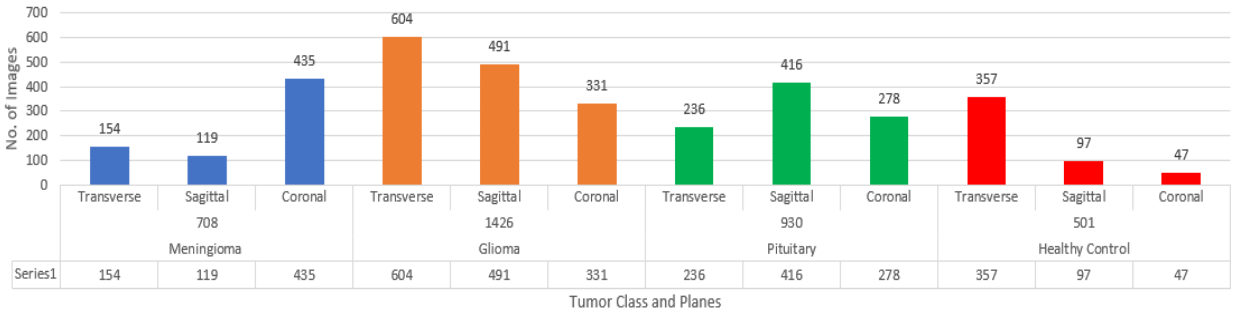

Fig 3.4. No of slices present in each category and views

3.2 BRAIN TUMOR CLASSIFICATION

For Detection of Tumor Type and its corresponding ICD Code, we have developed a classification model, for which the proposed methodology is given below in Figure 3.5.

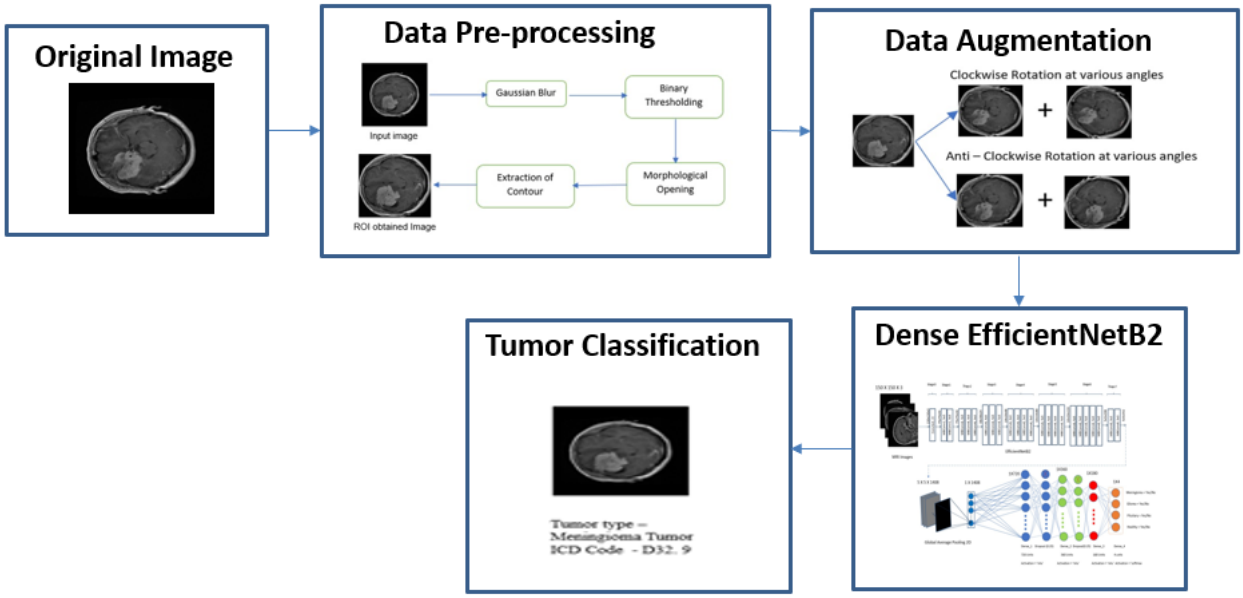

Fig 3.5. Overview of proposed methodology for brain tumor classification

3.2.1 DATA PRE – PROCESSING

The proposed method consists of extraction of the required image and mask according to their labels and a series of image processing methods to crop out the excess background whilst keeping only the part required ie. To extract the Region of Interest (ROI). This is done to improve the efficiency of training. Figure 3.6 shows the data pre – processing steps.

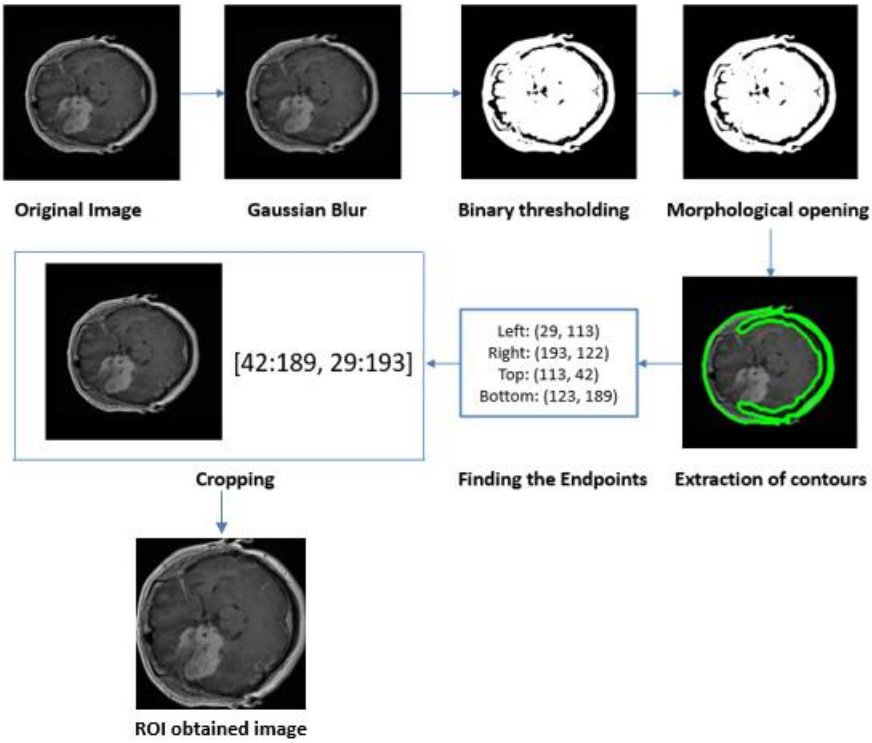

Fig 3.6. Overview of obtaining ROI image

First, the extracted image is converted to greyscale. Then, the Image is blurred a bit using Gaussian Blur to reduce image noise. Afterwards, Binary threshold is applied to get a binary image based on setting a threshold value on the pixel intensity of the original image. The pixel intensity here is set from 45 to 255. Next, we find the shapes required for our model training using find contour and the contours are grabbed. Finally, we extract the contour position from left, right, top and bottom, and using the extracted contours, a new image is generated in which the excessive background is removed and only the part which is needed to detect tumor is kept. The below figure 3.7 shows the original Image and the ROI extracted image.

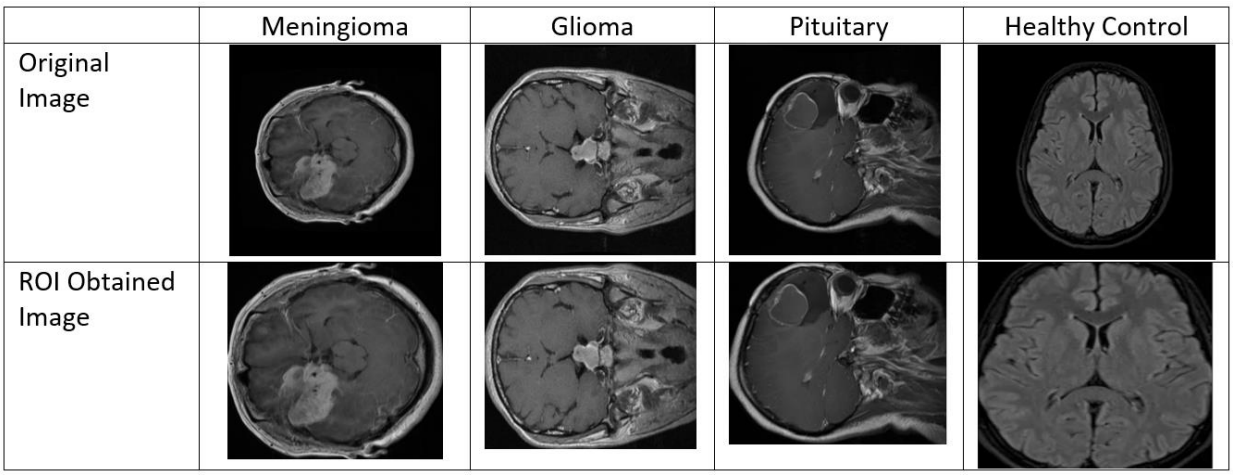

Fig 3.7. Original and ROI obtained MR images of each label

3.2.2 DATA AUGMENTATION

The deep neural network needs large datasets for better results, but the dataset is limited. The dataset contains 3565 brain images, further divided into 80% for training, and 20% which remains for testing and validation purposes. The dataset is also heavily misbalanced between each class which can impact the training accuracy. So, data augmentation is needed to change in the minor. We have applied rotation for each class separately for the data requirement.

We have rotated every single image in glioma tumor one time by 5 degrees counter clockwise, pituitary tumor two times by 5 degrees clockwise and counter clockwise and meningioma tumor three times by 5 degrees clockwise, counter clockwise also with 6 degrees counter clockwise and augmented them with the original image. This will enhance the amount of training data, allowing the model to learn more effectively. This may assist in increasing the quantity of relevant data. It contributes to the reduction of overfitting and enhances generalization. Data augmentation (DA) is the process of creating additional samples to supplement an existing dataset via transformation. By data warping or oversampling, this augmentation exaggerated the size of the training dataset. Figure 3.8 shows the Data Augmentation done for Brain tumor Classification.

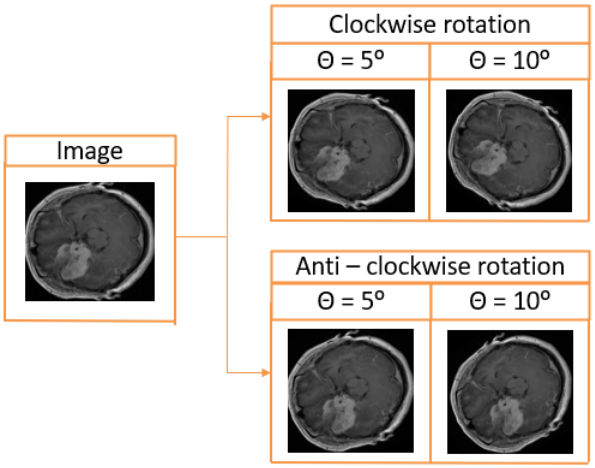

Fig 3.8. Data augmentation for brain tumor classification

Table 3.4 and Fig 3.9 shows the number of images present across each classes of tumor along with their planes and the corresponding images present along them after data augmentation.

Table 3.4. No of slices present in each category and views after data augmentation

Tumor Category	**No. of Slices**	**View**	**No. of Slices**
Meningioma	2832	Transverse	616
		Sagittal	476
		Coronal	1740
Glioma	2852	Transverse	1208
		Sagittal	982
		Coronal	662
Pituitary	2790	Transverse	708
		Sagittal	1248
		Coronal	834
Healthy Control	2505	Transverse	1785
		Sagittal	485
		Coronal	235

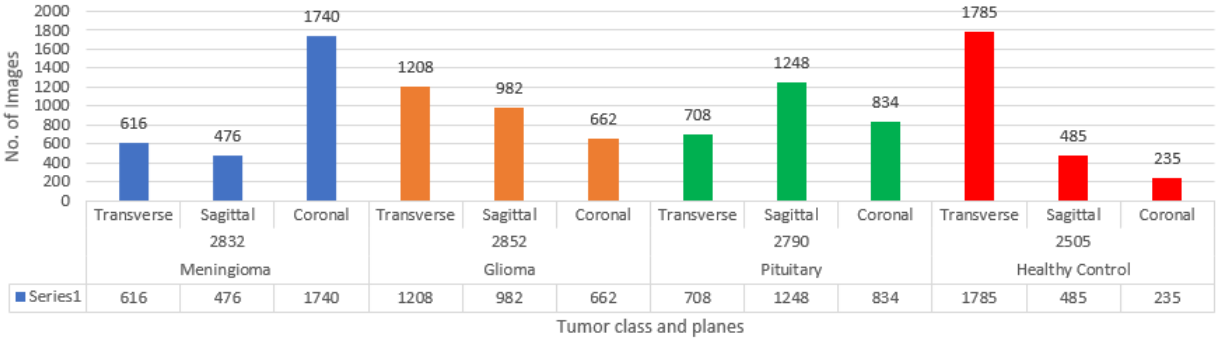

Fig 3.9. No of slices present in each category and views after data augmentation

3.2.3 MODIFIED EFFICIENT NET B2

Before seeing about modified efficientnet B2, let us know about what is efficientnet, its modules, sub – blocks and the architecture of efficientnet b2 first. Efficientnet is a convolutional neural network architecture and scaling method that uses a compound coefficient to scale all depth/width/resolution dimensions evenly. Unlike standard practise, which adjusts these factors randomly, the efficientnet scaling method consistently increases network breadth, depth, and resolution with a set of pre-set scaling coefficients [21]. Efficientnet scales up models with the help of a simple but effective technique known as compound coefficient. Instead of scaling up width, depth, or resolution at random, compound scaling scales each dimension equally with a given set of scaling coefficients [21]. To design the compound scaling method, the authors evaluated the effects of each scaling methodology on the model's performance and efficiency. While scaling single dimensions improves model performance, they reasoned that balancing the scale in all three dimensions (width, depth, and image resolution) improves overall model performance the most [39].

Let us now look into our architecture of modified efficient net b2. This paper presents a novel dense CNN model that combines pre-trained efficientnetb2 with dense layers. The dense block concept is made up of convolution layers the same size as the efficientnet input feature maps. Dense block uses the output feature maps of the preceding convolution layers to generate more feature maps with fewer convolution kernels.

The modified efficientnet network has two layers: dense and drop-out. A dense layer is the basic layer that feeds all of the previous layer's outputs to all of its neurons, with each neuron providing one output to the next layer. The drop-out layer is used during training to reduce capacity or thin the network and avoid overfitting. The model begins by addition of a pooling layer followed by three dense layers and two drop-out layers to ensure the model runs smoothly. The numbers of neurons in the dense units are 720, 360, and 180, respectively. The drop-out values are 0.25, and 0.25 respectively. Finally, we have used a dense layer composed of four fully connected neurons in conjunction with a Softmax output layer to compute and classify the probability score for each class. Figure 3.10 illustrates the structure of the proposed efficientnet in detail.

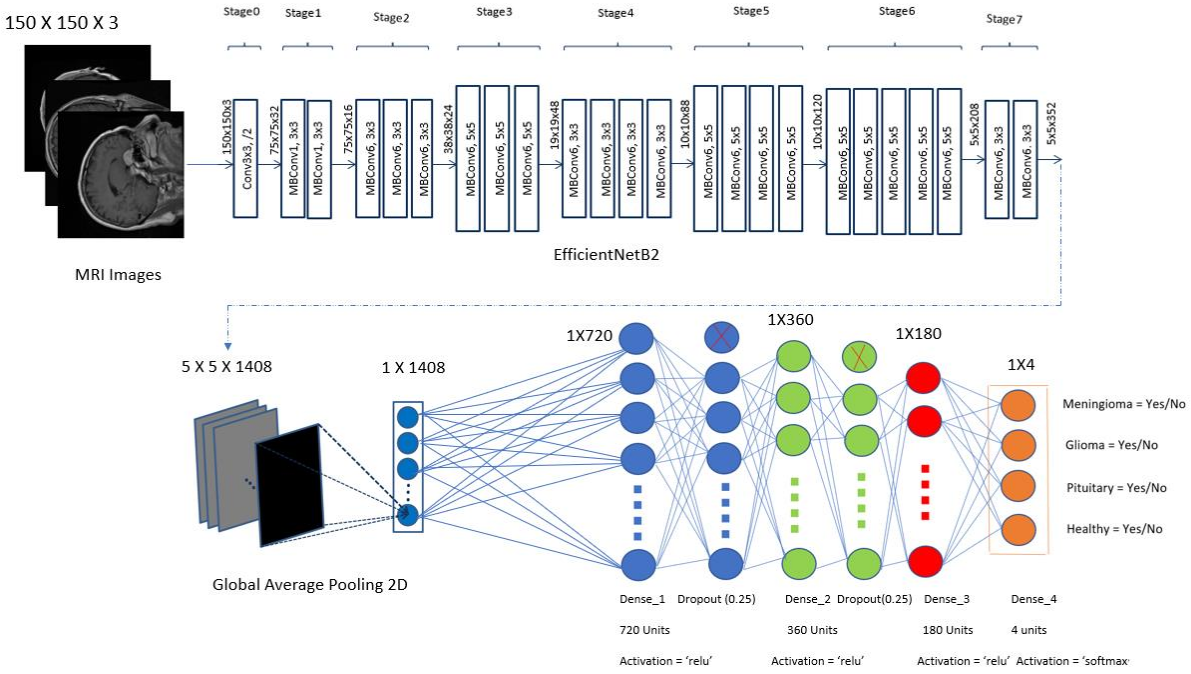

Fig 3.10. Proposed Modified Efficient Net B2 CNN Model Architecture

3.2.4 HYPERPARAMETERS SET AND OUTPUTS GENERATED

Table 3.5. Hyperparameters set for modified efficientnet b2

Hyperparameters	Values
Batch size	32
Epoch	20
Initial learning rate	0.0001
Reducing LOR at patience	2
Reducing LOR at factor	0.3
Optimizer	Adam

Table 3.5 shows the hyperparameters set for our modified efficientnet b2 to get the maximum accuracy.

The outputs generated are tumor type and the corressponding ICD code for that tumor type which will be visible on the report.

3.3 BRAIN TUMOR SEGMENTATION

For obtaining tumor radiomic characteristics, which is nothing but the tumor diameter and area, along with the original image with tumor region highlighted, we have developed a segmentation model, for which the proposed methodology is given below in Figure 3.11.

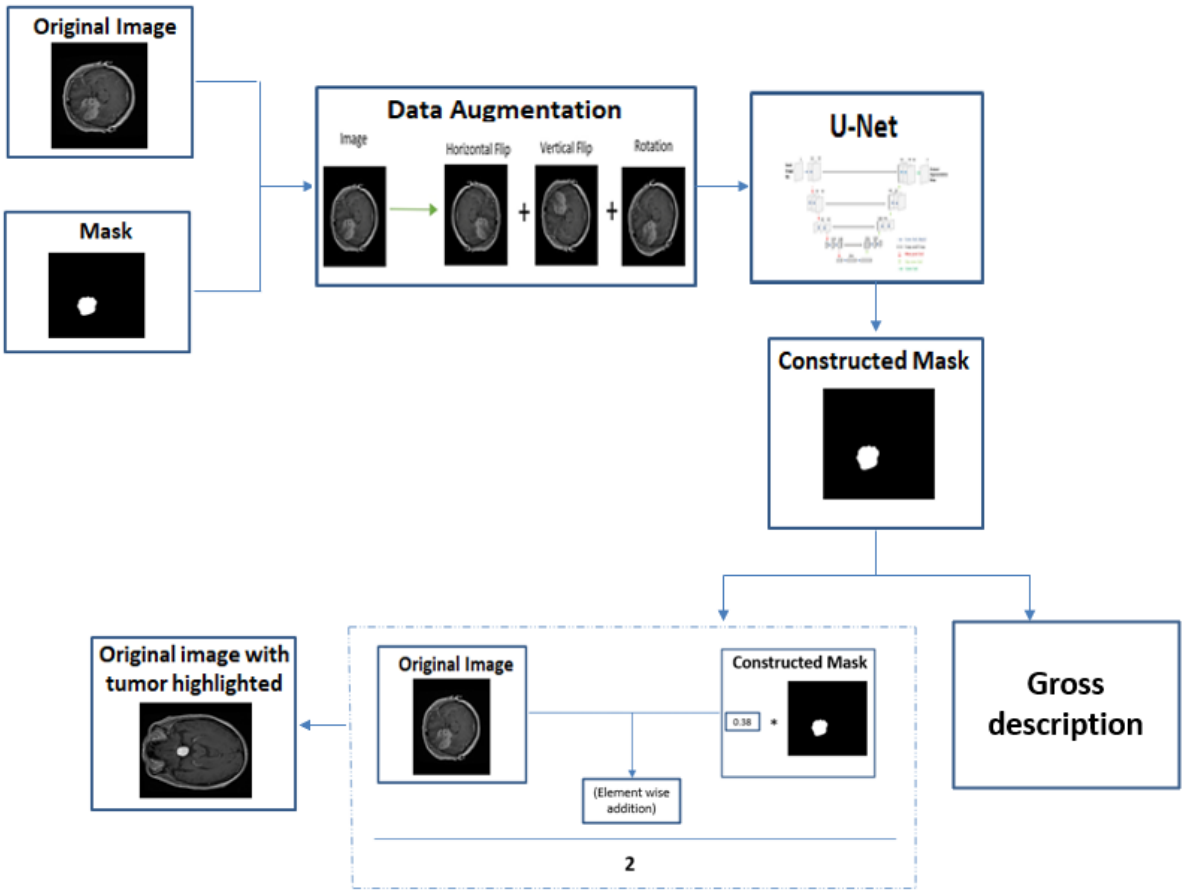

Fig 3.11. Overview of proposed methodology for Brain Tumor Segmentation

3.3.1 DATA AUGMENTATION

To diversify the training data, the basic forms of data augmentation are used. The torchvision module of Pytorch is used for all augmentation methods. They are as follows: horizontally flip, vertically flip, and rotate between 75 and -15 degrees. Each augmentation method has a probability of 0.5, and the order in which they are applied is also random. The degree of rotation for rotation augmentation is chosen at random between 75 and -15 degrees. Data augmentation for brain tumour segmentation is shown in Figure 3.12. The dataset is split in the ratio 80:20, where 80% is used for training the model and 10% is used for validation and 10% is used for testing. A total of 18384 images (9192 images and mask respectively) were obtained which will be utilized for the brain tumor segmentation.

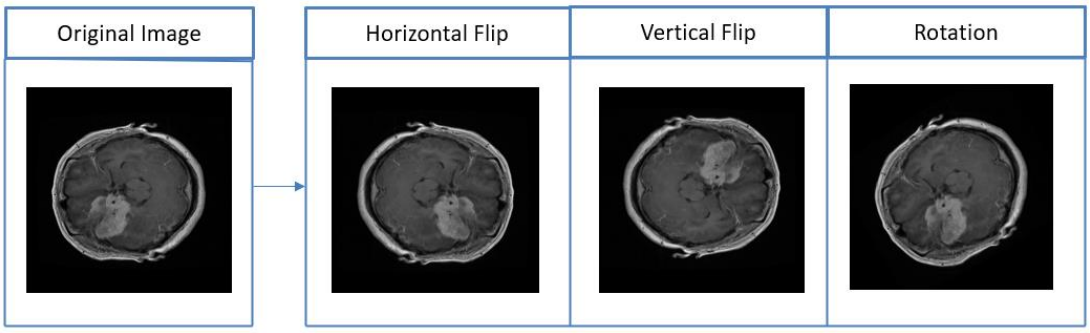

Fig 3.12. Data Augmentation for Brain Tumor Segmentation

Table 3.6 and Fig 3.13 shows the number of images present across each classes of tumor along with their planes and the corresponding images present along them after data augmentation.

Table 3.6. No of slices and its mask present in each category and views after data augmentation

Tumor Category	No. of Slices	View	No. of Slices
Meningioma	4248	Transverse	924
		Sagittal	714
		Coronal	2610
Glioma	8556	Transverse	3624
		Sagittal	2970
		Coronal	1986
Pituitary	5580	Transverse	1416
		Sagittal	2496
		Coronal	1668

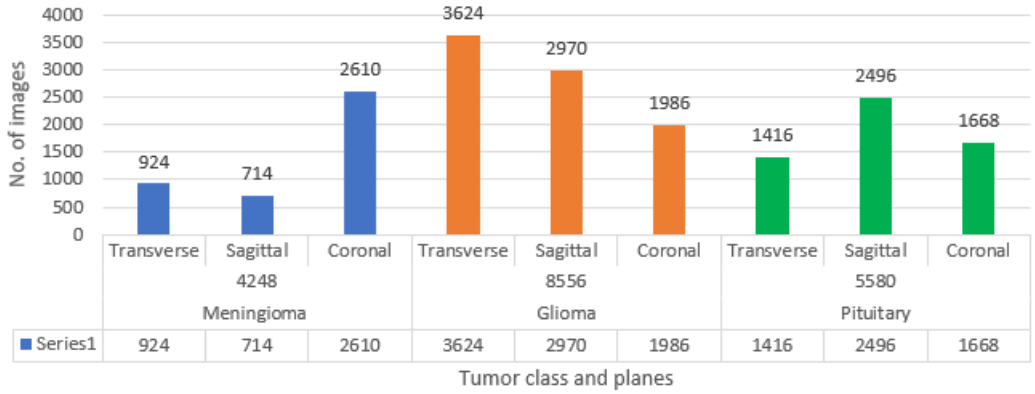

Fig 3.13. No of slices present in each category and views after data augmentation

3.3.2 U – NET

Olag Ronneberger et al. [40] introduced the U – net architecture for biomedical image segmentation. The resulting network is applicable to various biomedical segmentation problems. The architecture for U – net is given below in Figure 3.14.

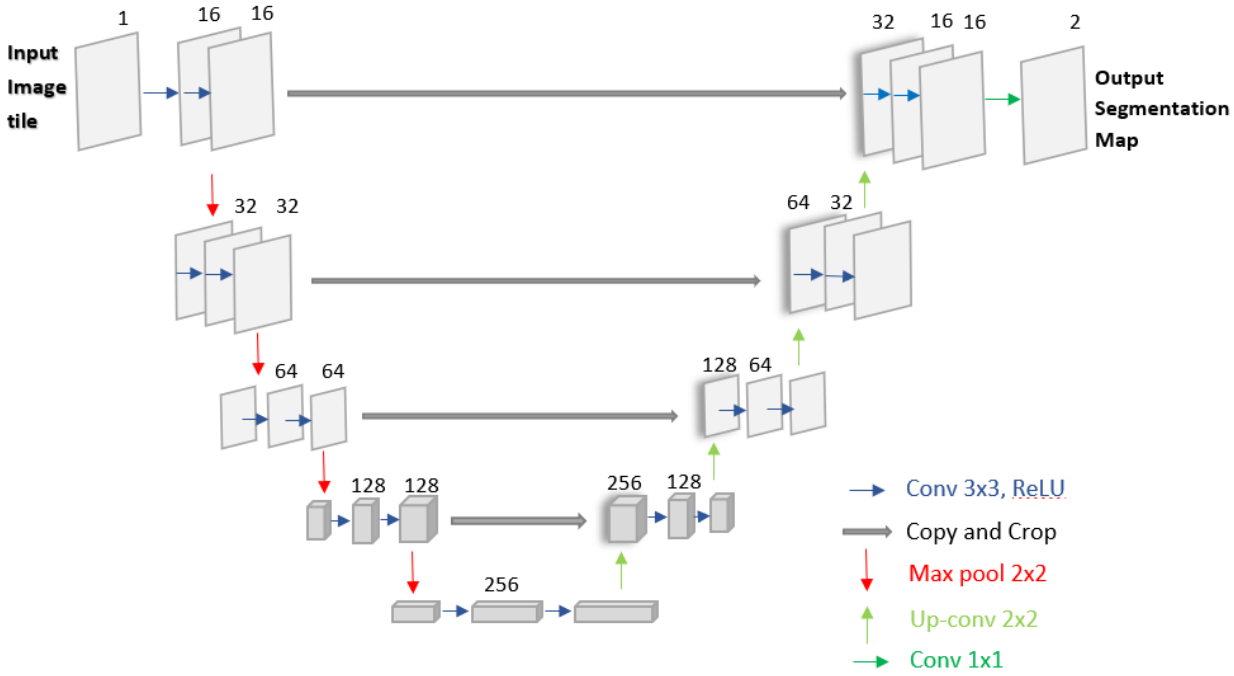

Fig 3.14. Architecture of U – Net [39]

The network architecture is made up of a contracting path (on the left side) and an expansive path (on the right side). The contracting path is designed in the manner of a convolutional network. It is composed of two 3x3 convolutions (unpadded convolutions) applied repeatedly, each followed by a rectified linear unit (ReLU) and a 2x2 max pooling operation with stride 2 for downsampling. We double the number of feature channels with each downsampling step. Every step in the expansive path begins with an upsampling of the feature map, followed by a 2x2 convolution ("up-convolution") that cuts the number of feature channels in half, a concatenation with the correspondingly cropped feature map from the contracting path, and two 3x3 convolutions, each followed by a ReLU. Because of the loss of border pixels in each convolution, cropping is required. A 1x1 convolution is used at the final layer to map each 16-component feature vector to the desired number of classes. The network has a total of 23 convolutional layers. To enable seamless tiling of the output segmentation map, the input tile size must be chosen so that all 2x2 max-pooling operations are applied to a layer with an even x- and y-size.

3.3.3 HYPERPARAMETERS SET AND OUTPUTS GENERATED

Table 3.5. Hyperparameters set for U – net

Hyperparameters	**Values**
Batch size	6
Epoch	100
Filters	[16, 32, 64, 128, 256]
Initial learning rate	0.001
Reducing LOR at patience	2
Reducing LOR at factor	0.85
Optimizer	Adam

Table 3.5 shows the hyperparameters set for our U – net to get the maximum accuracy.

A mask of the tumor will be generated using our U – net which will be utilized to find the outputs required for the tumor radiomic characteristics which are all given below.

3.4 TUMOR RADIOMIC CHARACTERISTICS

Radiomics is a quantitative approach to medical imaging, which provides a non-invasive approach to reliably extract quantitative features from radiographic images. The resulting features can be used to inform imaging diagnosis, prognosis, and therapy response [41].

The above U – Net model is used by us for training our dataset and hence constructing a mask using the model for the images which we give as input as shown in Figure 3.15.

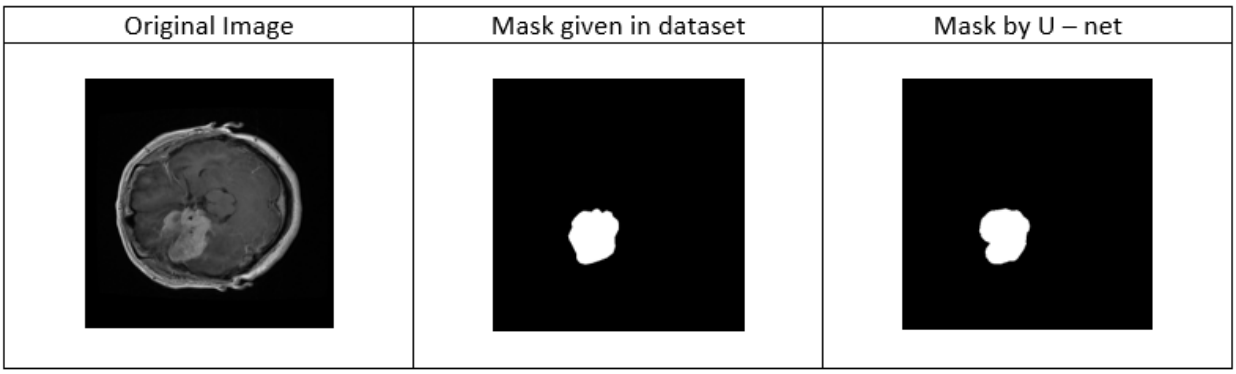

Fig 3.15. Original image, mask given in the dataset and the mask built by U – net.

Using the above mask generated from our U – net, we can obtain the following outputs required to generate a preliminary diagnostic report of the brain tumor as shown in Figure 3.16.

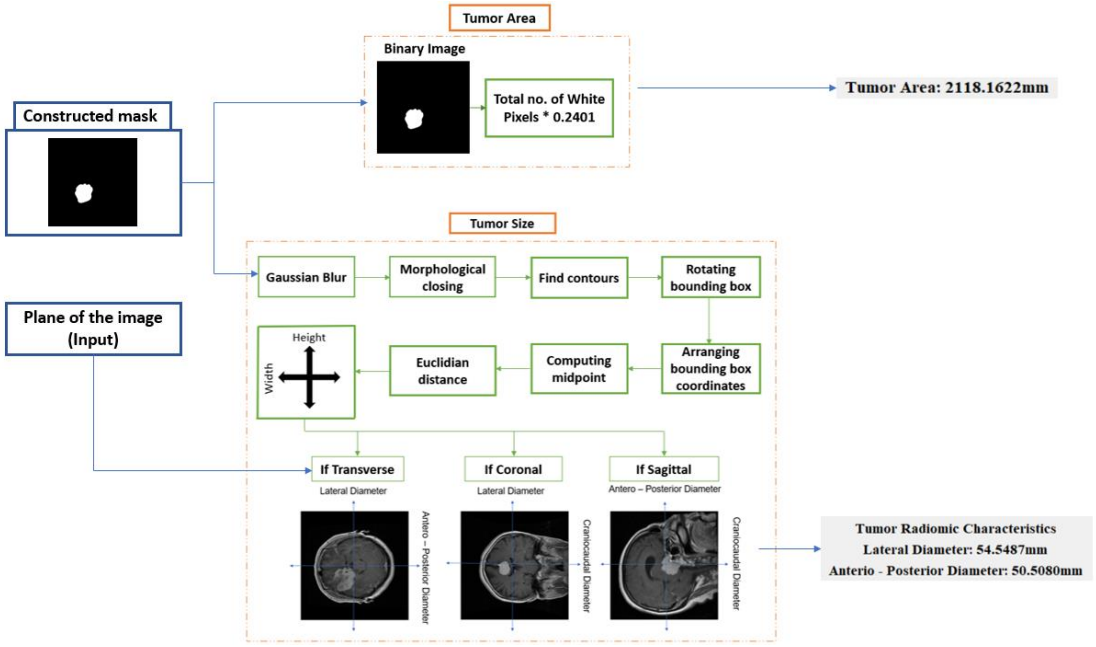

Fig 3.16. Overview of proposed methodology for obtaining the Tumor Radiomic Characteristics

For better visualization of the tumor, we can highlight the tumor in the original image by multiplying the mask generated by our U – net with a certain transparency range. Transparency level varies between 0 to 1 with 0 being complete transparent and 1 being complete opaque.

We fixed the transparency range at 0.38 as this is optimal for visualization of the tumor. The multiplied mask generated by our U – net output is then added with the original image arguments element wise and then divided by 2 to obtain the final output shown below in figure 3.17.

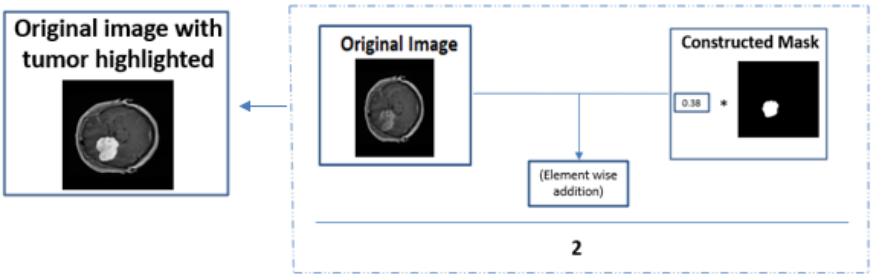

Fig 3.17. Procedure to obtain original image with tumor highlighted

Tumor diameter is defined as the maximal size of the invasive component of the primary tumor on pathologic examination.

Tumor diameter is found by finding the contours in the mask generated by our U – net and using the contours we find the bounding box, and then unpack the ordered bounding box, then compute the midpoint between the top-left and top-right coordinates, followed by the midpoint between bottom-left and bottom-right coordinates. Using these midpoints, we find the Euclidian distance between these points. These points are multiplied with 0.49, where the pixel value is 0.49mm [19], thus getting the tumor diameter.

We can obtain three different diameters of the tumor using only two different oriented images. The three different diameters are:

Craniocaudal Diameter (d_{cc}) – along the long axis of the endometrial cavity

Antero – Posterior Diameter (d_{ap}) – along the anterior and posterior side of our brain

Lateral Diameter (d_l) – along the lateral side of our brain

We can obtain craniocaudal diameter from either sagittal or coronal plane, antero – posterior diameter from either transverse or sagittal plane and lateral diameter from either transverse or coronal plane. By giving the image and the orientation of the image as input, we can obtain the diameters of the tumor as shown below in figure 3.18.

Tumor area is calculated by converting the mask generated by our U – net into a binary image, taking the total count of the white pixels in the region, and multiplying it by 0.49 * 0.49 mm [36].

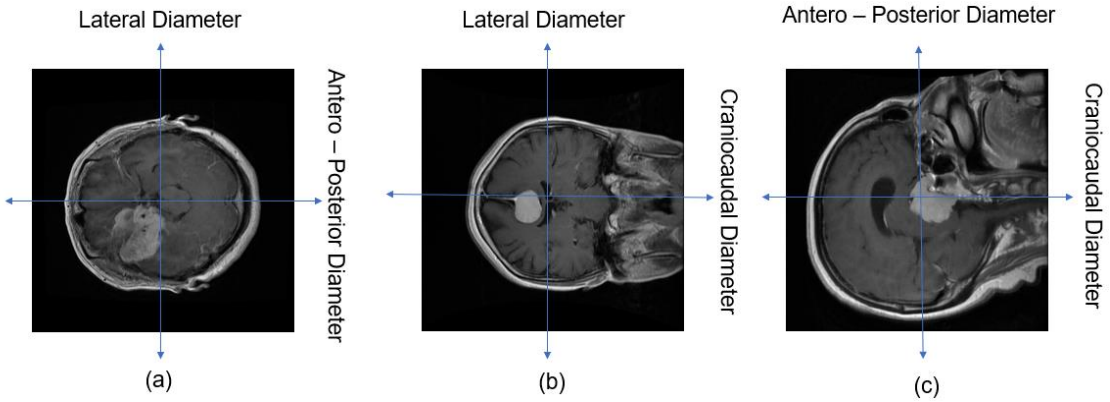

Fig 3.18. (a) Transverse Plane and it's Diameter, (b) Coronal Plane and it's Diameter, (c) Sagittal Plane and it's Diameter

3.4.1 OUTPUTS GENERATED

The outputs generated are tumor diameter along with the tumor area which are all the tumor radiomic characteristics, which will be printed in the preliminary report.

3.5 PRELIMINARY REPORT GENERATION

A preliminary report will be generated automatically, in which it takes the following input as shown in Figure 3.19.

- Input Image (T1 – Weighted Contrast Enhanced MRI Images)
- Plane of the Input Image (Transverse or Sagittal or Coronal)

Fig 3.19. Inputs Given for Report Generation

The following outputs will be generated in the preliminary report.

- Original image with tumor highlighted
- Tumor type and its ICD code
- Tumor diameter
- Tumor area Fig 3.20 shows the following outputs generated in the preliminary report

Fig 3.20 shows the algorithm behind the preliminary report generation. First, we get input from user which is then fed into our classification algorithm, using that we get the tumor type. If the tumor type is none (i.e.) Healthy, then the whole segmentation algorithm process is skipped, and the tumor radiomic characterisitics will be displayed as "NA" in the output, else then the segmentation and tumor radiomics algorithm process will be gone through from which we will get the tumor radiomic characterisitcs (i.e.) tumor diameter and area in our preliminary report.

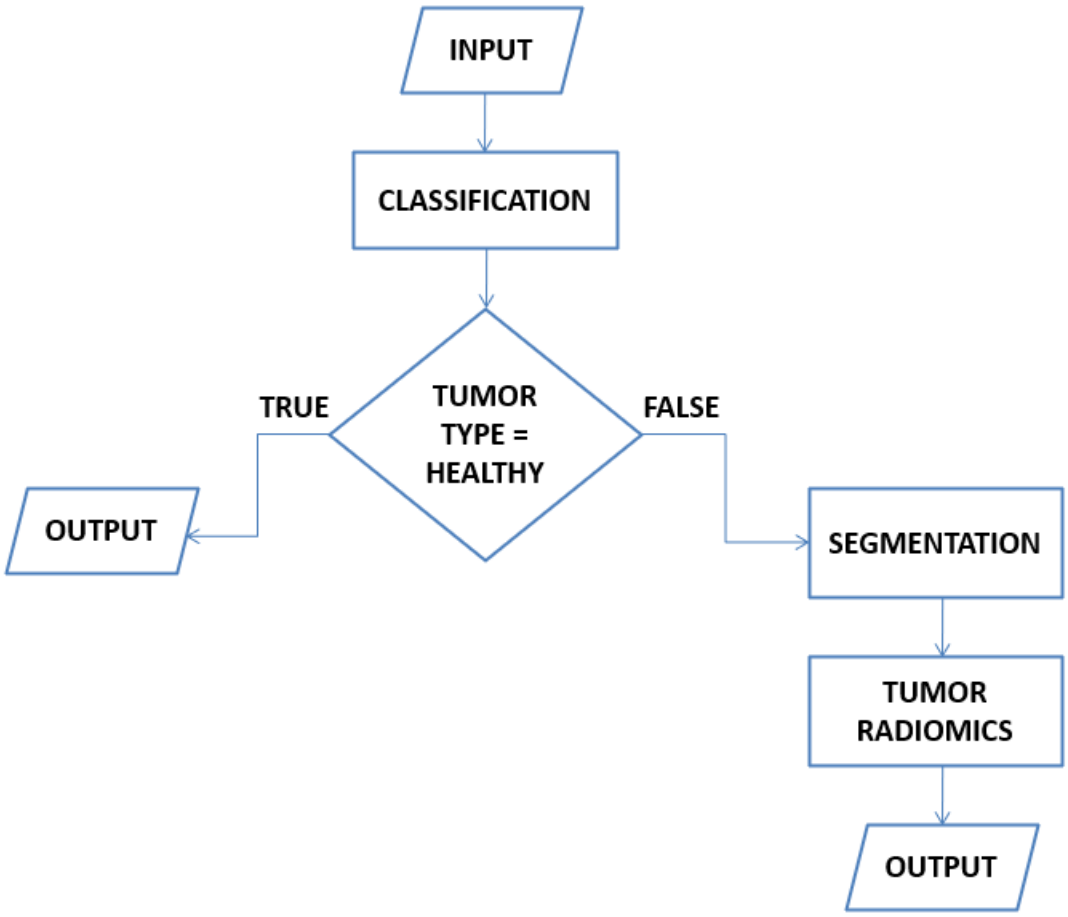

Fig 3.20. Algorithm for Preliminary report generation

Fig 3.21 shows the following outputs generated in the preliminary report.

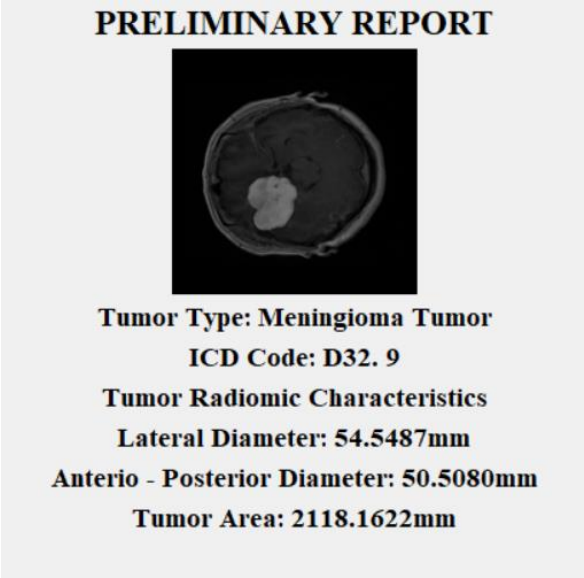

Fig 3.21. An example of output in the Preliminary Report

The Input text box and button GUI is designed using Python Tkinter for user convinience. The standard Python interface to the Tcl/Tk GUI toolkit is the tkinter package ("Tk interface"). Tk and tkinter are both available on most Unix platforms, including macOS, as well as Windows. [42]. One primary widgets were used here for our project in Tkinter and one from PIL module. They are: tkinter.label and PIL.Imagetk respectively. tkinter.label is a widget that is used to implement display boxes where you can place text or images. The ImageTk module contains support to create and modify Tkinter BitmapImage and PhotoImage objects from PIL images. Fig 3.22 shows the entire preliminary report.

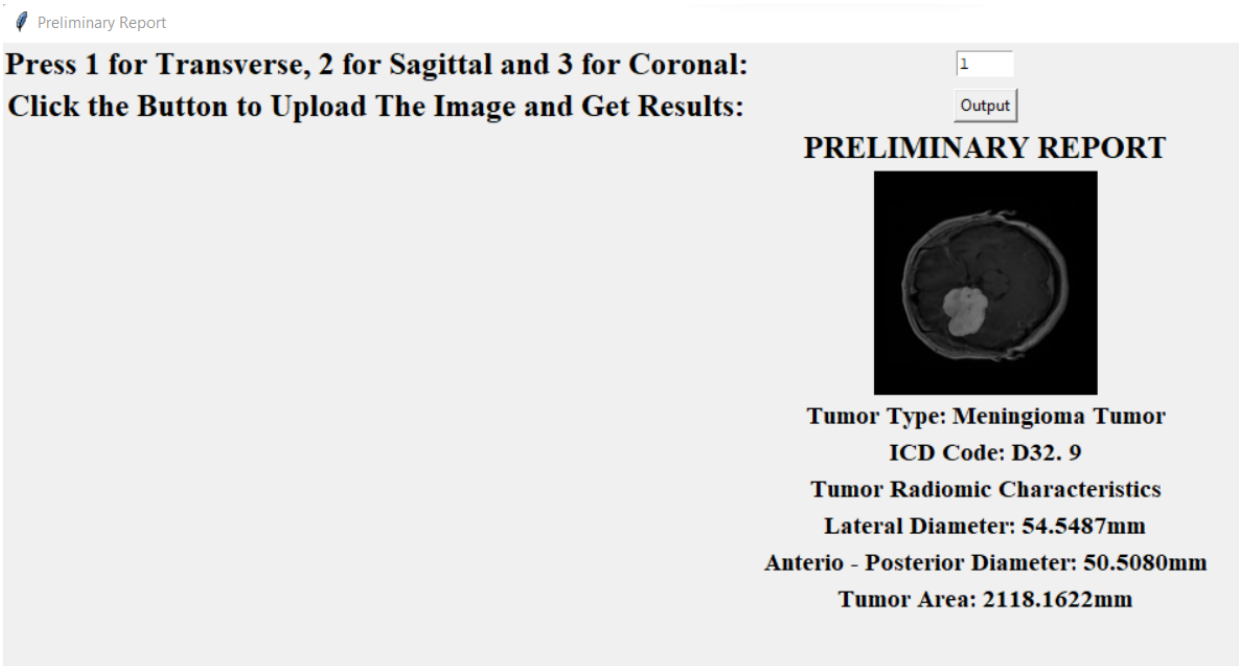

Fig. 3.22 Preliminary Report

CHAPTER 4

RESULTS AND DISCUSSION

This chapter discusses about the performance of the models used for detection and diagnosis of brain tumor using MRI Images. Two models, Modified EfficientNet B2 which is used for classification of brain tumor therby finding Tumor type and its ICD Code and UNet which is used for brain tumor segmentation therby generating a mask which can be used to find Tumor Diameter and Tumor area are prepared using the same dataset. The model training is done using google colab and the preliminary report generatio is done using python and tkinter. The evaluation of both models is done using various model validation techniques given below.

4.1 BRAIN TUMOR CLASSIFICATION

4.1.1 LOSS AND ACCURACY

Several experimental tests have been performed to determine the validity of the proposed dense CNN model. All of the experiments were carried out in a Python programming environment with GPU support. Pre-processing is performed first, in which the images are cropped for better training and then augmented for training. Accuracy is defined as the ratio of correct predictions to total samples. To improve accuracy, the proposed model activated the augmented tumors. The proposed model showed 99.93% accuracy on training data and 97.63% accuracy on the testing dataset which is plotted in Figure 4.2

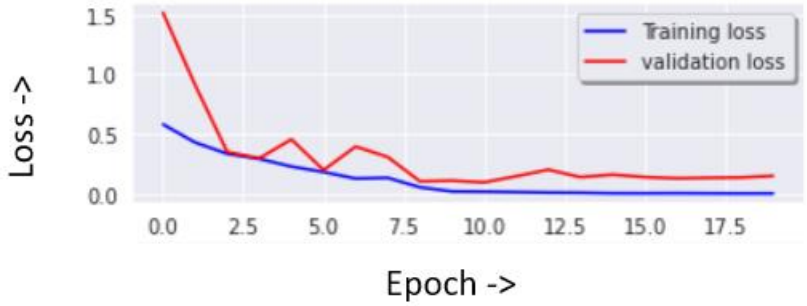

Fig 4.1. Loss Plot

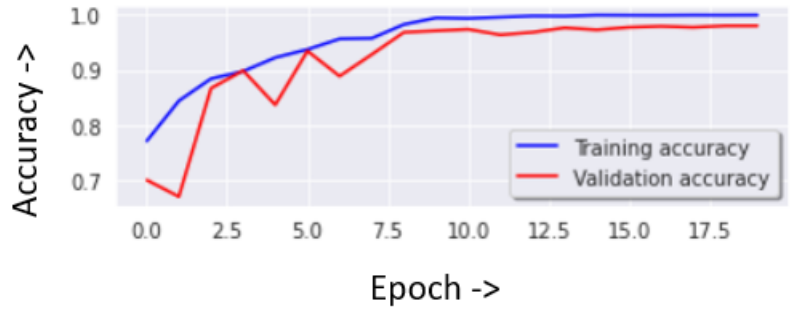

Fig 4.2 Accuracy Plot

The experiment has been performed in 20 epochs. A batch size of 32, image size 150 x 150, and verbose 1 have been considered for the experiment. In the accuracy model shown in above figure 4.2, initial validation accuracy is around 0.7013 but after two epochs the validation accuracy suddenly increases to nearly 0.8670.

In the same manner, as seen in figure 4.1, the initial validation loss is 1.1516 but after two epochs the loss decreases to 0.3502. As shown in Figure 4.1 and 4.2, there is a positive trend toward improving accuracy and reducing loss. At first, validation accuracy is low, but it progressively improves to almost 97 percent. The testing accuracy and testing loss of modified EfficientNetB2 is 97.63% and 0.1493 respectively.

4.1.2 CONFUSION MATRIX

To compare the performance of the proposed model, various performance measures such as accuracy, precision, recall, and F1-score were used. The confusion matrix was used to evaluate these parameters. The details were also examined using the confusion matrix which is shown below in Figure 4.3. For comparison of different techniques, three important measures have been considered: precision, recall, and F1-score. All these measures are based on the following parameters:

True positive (TP) - A test result that correctly indicates the presence of a condition or characteristic [43].

True negative (TN) - A test result that correctly indicates the absence of a condition or characteristic [43].

False positive (FP) - A test result which wrongly indicates that a particular condition or attribute is present [43].

False negative (FN) - A test result which wrongly indicates that a particular condition or attribute is absent [43].

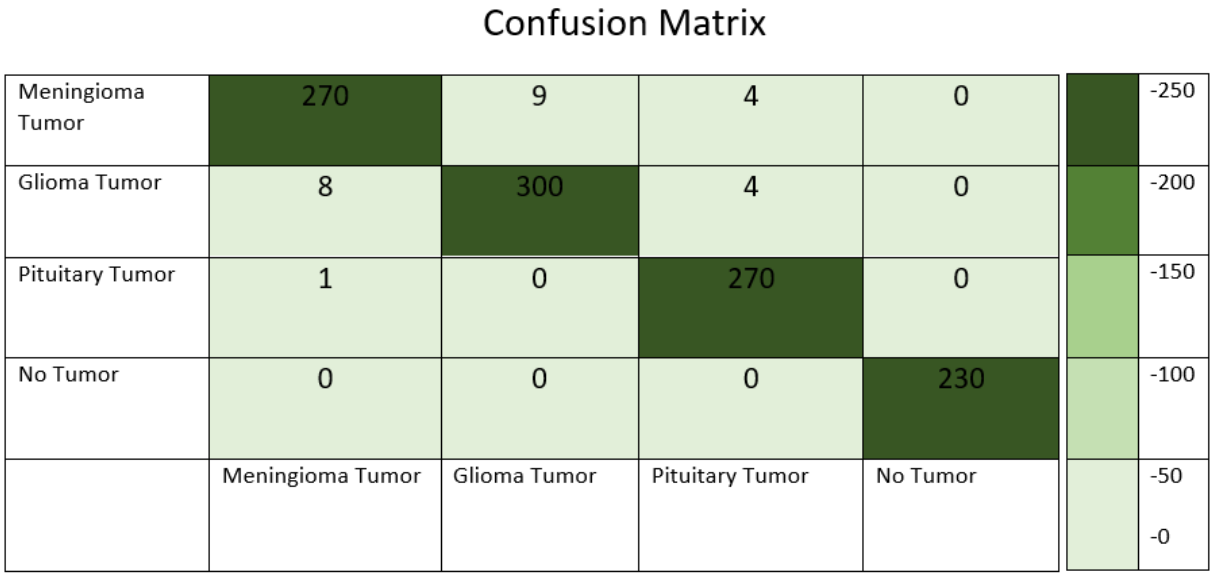

Fig 4.3. Confusion Matrix of the Modified Efficient Net B2

The confusion matrix presents misclassifications because of overfitting using 10% of testing data obtained from the original dataset. From the matrix it is observed that the misclassified tumors in the proposed modified EfficientNet B2 is 9 out of 1096 testing images. Due to lesser amounts of misclassified data, the accuracy of the proposed model is higher than the others. Most of the misclassified samples belong to the ”meningioma” class which cannot learn as effectively as the other three.

4.1.3 CLASSIFICATION REPORT

For comparison of different techniques, three important measures have been considered: precision, recall, and F1-score. The definition for the measures and the evaluation of these measures for our model is given below:

Precision: The precision is determined by dividing the number of correctly classified Positive samples by the total number of Positive samples (either correctly or incorrectly). The precision of the model indicates how accurate it is at classifying Positive samples. [43].

$$\text{Precision} = \frac{\text{TruePositive}}{\text{TruePositive} + \text{FalsePositive}} \quad \text{---------- (1)}$$

Recall: The recall is calculated by dividing the total number of Positive samples by the percentage of Positive samples correctly classified as Positive. The recall measures the model's ability to recognise Positive samples. The greater the recall, the more positive samples discovered. [43].

$$\text{Recall} = \frac{\text{TruePositive}}{\text{TruePositive} + \text{FalseNegative}} \quad \text{---------- (2)}$$

F1-Score: The F1-score is a model accuracy metric that determines how accurate a model is on a given dataset. It is the harmonic mean of the model's precision and recall, and it is a method of combining the model's accuracy and recall [43]. A perfect model has an F-score of 1.

$$\text{F1 Score} = \frac{2}{\frac{1}{\text{Recall}} * \frac{1}{\text{Precision}}} \quad \text{---------- (3)}$$

Figure 4.4 shows the classification report of the modified efficientnet b2

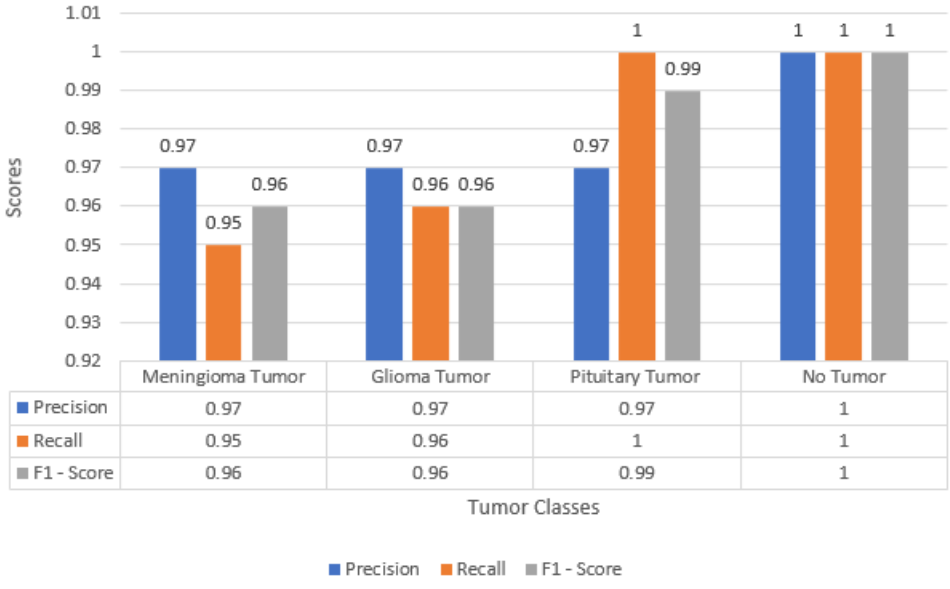

Fig. 4.4. Classification Report

It is observed from Table 4.1 that Modified EfficientNetB2 has the highest precision, recall, and F1-score when compared with other models given below. The no tumor has the best performance in all measurements when compared to other types of tumors. All the values of precision, recall, and F1-score of pituitary tumors are quite good. The overall results of the modified EfficientNetB2 are excellent.

For comparison purposes, we also considered the most recent performance of modified CNN structures by various researchers., which is shown in Table 4.1. The accuracy, precision, and F1-score of the proposed method are 97.63%, 98%, and 98%, respectively, which is better than other comparison methods. As shown in Table 4.2, Deep learning segmentation algorithms proposed here outperform state-of-the-art techniques. Based on Table 4.1, we conclude that modified EfficientNet B2 outperforms other techniques because deep-learning-based approaches are more efficient and capable of handling large amounts of data for classification.

Table 4.1. Comparison of performance among different deep-learning-based techniques

AUTHORS	**YEAR**	**DATASET**	**MODEL**	**ACCURACY**	**PRECISION**	**F1-SCORE**
Badza et al [25].	2020	T1 contrast brain tumors [37]	CNN	96.56%	94.81%	94.94%
Mizoguchi et al [44].	2020	Brats-2018 [52]	3D-CNN	96.49%	-	-
Hashemzehi et al [45].	2020	T1 contrast brain tumors [37]	CNN and NAND	96.00%	94.49%	94.56%
Díaz-Pernas et al [29].	2021	T1 contrast brain tumors [37]	Multi-scale CNN	97.00%	95.80%	96.07%
Sajja et al [46].	2021	T1 contrast brain tumors [37]	Deep-CNN	96.70%	97.05%	97.05%
Proposed method	2022	T1 contrast brain tumors [37]	Modified Efficient Net B2	97.63%	98%	98%

4.1.4 DISCUSSION

Table 4.2 and figure 4.5 shows the accuracy of our model at each plane and the class of the tumor.

Table 4.2. Accuracy for each plane of the image and tumor class

Image Plane	Accuracy	Tumor Class	Accuracy
Transverse	98.84%	Meningioma	96%
		Glioma	98%
		Pituitary	99%
		Healthy	100%
Sagittal	99.29%	Meningioma	98%
		Glioma	99%
		Pituitary	100%
		Healthy	100%
Coronal	99.42%	Meningioma	99%
		Glioma	99%
		Pituitary	99%
		Healthy	100%

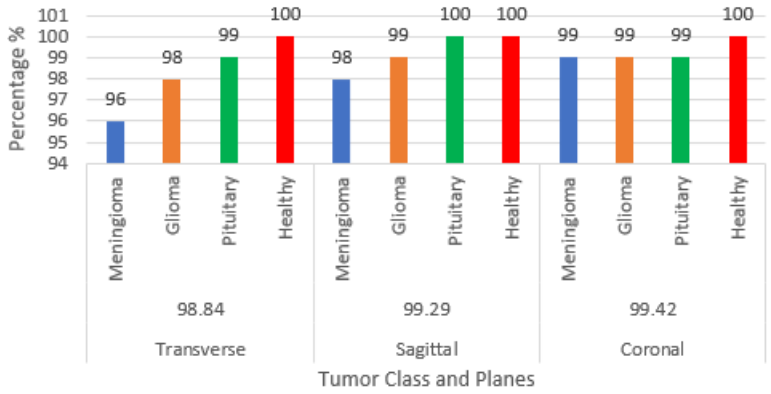

Fig 4.5. Accuracy for each plane of the image and tumor class

We can see from the table that our model performs best in coronal plane wheras it performs comparatively less in transversal plane. This might be due to misbalancing of the data between classes being comparatively higher in transversal plane than in coronal plane. We can also see that healthy control images performs the best when comparing to other classes. This is due to the healthy control image having no tumor inside them which makes them easy to distinguish. Meningioma and Glioma class has lower percentage when comparing to pituitary and healthy control. Among the three types of tumor classes, Pituitary performs the best and meningioma performs comparitively less. This is due to meningioma class having less data when comparing to pituitary class.

4.2 BRAIN TUMOR SEGMENTATION

4.2.1 LOSS PLOT

The training is run on google colab with the single 12GB NVIDIA Tesla K80 GPU [47] that can be used up to 12 hours continuously. Total time taken for model training was 6 hours and 30 minutes. We started with an initial learning rate of 1e-3 and reduced it by 85% on plateauing, final learning rate at the end of 100 epochs was 2.7249e-4. The graph indicating Loss Value over 100 epochs are given below in Figure 4.6.

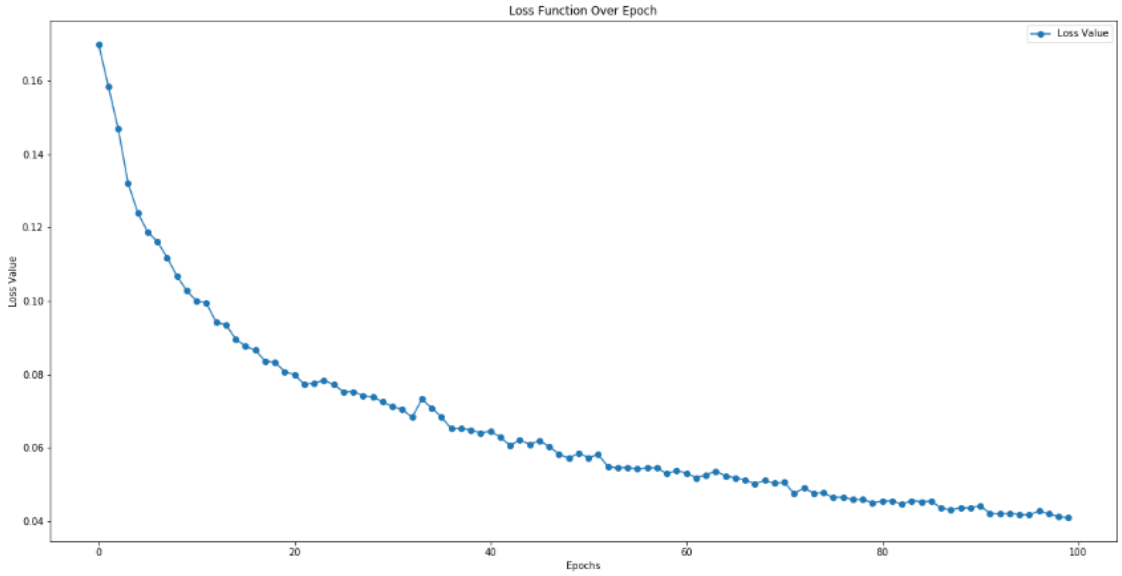

Fig 4.6. Loss Plot

4.2.2 SORENSEN – DICE COEFFICIENT

The Dice score is often used to quantify the performance of image segmentation methods. There, annotation of some ground truth region in the image is done and then an automated algorithm is made to do it. The validation of the algorithm is done by calculating the Dice score, which is a measure of how similar the objects are. So, it is the size of the overlap of the two segmentations divided by the total size of the two objects [48]. Using the same terms as describing accuracy, the Dice score is [48]:

$$\text{Dice Score} = \frac{2 * \text{TruePositive}}{2*\text{TruePositive} + \text{FalsePositive} + \text{FalseNegative}} \quad \text{---------- (4)}$$

The mean Dice Score the model gained was 0.7717 in testing dataset of 600 images. From this we can conclude that in our testing dataset, our generated mask from U – net has a similarity of about **77%** with the original mask.

4.2.3 STRUCTURAL SIMILARITY INDEX

The structural similarity index measure (SSIM) predicts the perceived quality of digital television and cinematic images, as well as other types of digital images and videos. SSIM is a tool for determining the similarity of two images [49].

The SSIM index is a full reference metric, which means that image quality is measured or predicted using an initial uncompressed or distortion-free image as a reference.

$$\text{SSIM}(x, y) = \frac{(2\mu_x\mu_y + C_1)(2\sigma_{xy} + C_2)}{(\mu_x^2 + \mu_y^2 + C_1)(\sigma_x^2 + \sigma_y^2 + C_2)} \quad \text{---------- (5)}$$

Where, $\boldsymbol{\mu_x}$ the average of **x**

$\boldsymbol{\mu_y}$ the average of **y**

$\boldsymbol{\sigma_x^2}$ the variance of **x**

$\boldsymbol{\sigma_y^2}$ the variance of **y**

σ_{xy} the covariance of **x** and **y**

$C_1 = (k_1L)^2$, $C_2 = (k_2L)^2$ two variables to stabilize the division with weak denominator.

L the dynamic range of the pixel-values (typically this is $2^{\#bits\ per\ pixel} - 1$)

$K_1 = 0.01$ and $k_2 = 0.03$ by default.

The mean SSIM the model gained was 0.9874 in testing dataset of 600 images.

4.2.4 MEAN SQUARE ERROR

The mean squared error (MSE) or mean squared deviation (MSD) of an estimator (of a procedure for estimating an unobserved quantity) in statistics measures the average of the squares of the errors—that is, the average squared difference between the estimated and actual values [50].

$$MSE = 1/n\ \Sigma i=1\ to\ n(Yi - \overline{Yi}) \quad \text{---------- (6)}$$

where, MSE = mean squared error

n = number of data points

Yi = observed values

$\overline{Yi}$ = predicted values

The mean square error the model gained was 0.006603 in testing dataset of 600 images

4.2.5 JACCARD INDEX

The Jaccard similarity index (also known as Intersection over Union (IoU)) compares members from two sets to determine which are shared and which are distinct. It is a measure of similarity between two sets of data, with a scale ranging from 0% to 100%. The higher the percentage, the closer the two populations are [51].

$$J(A, B) = \frac{|\ A \cap B\ |}{|\ A\ U\ B\ |} \quad \text{---------- (7)}$$

Where, J = Jaccard Similarity Index or Intersection over Union

A = Set1

B = Set2

The mean IoU the model gained was 0.6758 in testing dataset of 600 images

4.2.6 DISCUSSION

Table 4.4. Performance metrics of U – net in each classes

U – Net [16, 32, 64, 128, 256]			
Sorensen Dice Coefficient	Structural Similarity Index	Mean Square Error	Jaccard Similarity Index
0.7717	0.9871	0.006603	0.6758

Table 4.4 shows a summary of the various performance metrics of our U – Net model. Four different metrics were used for evaluation of our model. They are Sorensen Dice Coefficient, Structural Similarity Index, Mean Square Error and Jaccard Similarity Index. However, the main performance metrics which is most commonly used for evaluation of segmentation models is Sorensen dice coefficient, also known as dice score. Our model has gained a dice score of 0.7717. There is room for improving the model accuracy which can be achieved by changes in hyperparameters, using other models like nested U – net etc. But for this U – net, the hyperparameters set was optimal to our computational specification as we are limited by our computational capability.

CHAPTER 5

CONCULSION AND FUTURE WORKS

This chapter deals with the conclusions that is inferred from this project work. This report is of the project “Automated Detection and Diagnosis of Brain Tumor using MRI Images”.

In this project, we present an automated detection and diagnosis of brain tumor using MRI Images, where we build a system which automatically generates a preliminary report which contains the type of tumor, its corresponding ICD code, tumor diameter and tumor area along with the original input image with the tumor highlighted for visualization. This will be achieved through classification and segmentation of the MRI images, where the classification will be done to identify the tumor type and ICD code and segmentation will be done to visualize the tumor and to find its diameter and area. For our project, a preliminary report is being constructed which utilizes one MRI image of a brain tumor to diagnose the above criteria.

The major limitation of this project is in the accuracy of segmentation, which is only around 77%. There are algorithms like Unet++ [53] which gives an improved performance over the regular Unet but currently we are limited by our computational capability. Another way is to include more pre – processing steps like Contrast Limited Adaptive Histogram Equalization (CLAHE), which can also aid in improving the accuracy of the segmentation model. Another limitation lies in the fact that, the dataset which we had utilized lacks demographics details of the patient. This had limited our scope of the project to just diagnosing tumor diameter and area. Obtaining patient demographic details opens more scope for improvement in diagnosis of brain tumor, especially in finding of tumor volume and tumor growth rate.

Some scope for improvement can be done in adding more classes of brain tumor so that we can detect and diagnose more brain tumor diseases. The project only utilizes **.png** images which are not the medical standard for detection and diagnosis. Using .**dicom** images will be the medical standard.

Nowadays, the issue of automated detection and diagnosis of brain tumors are major research area. Our project, which is automating the process of detection, diagnosis and generation of a preliminary diagnosis report of the brain tumor will aid the radiologist and physician and will aid in more research work in the automation of the detection and diagnosis of brain tumor.

BIBILOGRAPHY

[1] "Brain - Wikipedia", *En.wikipedia.org*, 2022. [Online]. Available: https://en.wikipedia.org/wiki/Brain. [Accessed: 10- May- 2022].

[2] "Brain and Nervous System Part 2 - Pain & Posture Wellness Centre", *Pain & Posture Wellness Centre*, 2022. [Online]. Available: https://ppwc.co.uk/find-brain-nervous-system-work-part-2/. [Accessed: 10- May- 2022].

[3] P. Hartmann, A. Ramseier, F. Gudat, M. Mihatsch, W. Polasek and C. Geisenhoff, "Normal weight of the brain in adults in relation to age, sex, body height and weight", *Der Pathologe*, vol. 15, no. 3, pp. 165-170, 1994. Available: 10.1007/s002920050040 [Accessed 10 May 2022].

[4] A. Dekaban and D. Sadowsky, "Changes in brain weights during the span of human life: Relation of brain weights to body heights and body weights", *Annals of Neurology*, vol. 4, no. 4, pp. 345-356, 1978. Available: 10.1002/ana.410040410 [Accessed 10 May 2022].

[5] K. Jones, *Neurological assessment*. Edinburgh: Churchill Livingstone/Elsevier, 2011.

[6] FitzGerald MJT, Gruener G, Mtui E: Clinical neuroanatomy and neuroscience, St Louis, 2012, Elsevier, pp 78, 97–110, 299.

[7] "Brain Cancer Symptoms, Causes and Treatment in India - Apollo Hospitals", *Apollo Hospitals*, 2022. [Online]. Available: https://www.apollohospitals.com/departments/cancer/organ-cancer/brain-central-nervous-system/. [Accessed: 10- May- 2022].

[8] "Brain Tumor - Statistics", *Cancer.Net*, 2022. [Online]. Available: https://www.cancer.net/cancer-types/brain-tumor/statistics. [Accessed: 10- May- 2022].

[9] "Meningioma - Symptoms and causes", *Mayo Clinic*, 2022. [Online]. Available: https://www.mayoclinic.org/diseasesconditions/meningioma/symptoms-causes/syc-20355643. [Accessed: 10- May- 2022].

[10] "Glioma - Symptoms and causes", *Mayo Clinic*, 2022. [Online]. Available: https://www.mayoclinic.org/diseases-conditions/glioma/symptoms-causes/syc-20350251. [Accessed: 10- May- 2022].

[11] "Pituitary tumors - Symptoms and causes", *Mayo Clinic*, 2022. [Online]. Available: https://www.mayoclinic.org/diseases-conditions/pituitary-tumors/symptoms-causes/syc-20350548. [Accessed: 10- May- 2022].

[12] "Brain Tumor - Diagnosis", *Cancer.Net*, 2022. [Online]. Available: https://www.cancer.net/cancer-types/brain-tumor/diagnosis. [Accessed: 10- May- 2022].

[13] "International Classification of Diseases (ICD)", *Who.int*, 2022. [Online]. Available: https://www.who.int/standards/classifications/classification-of-diseases. [Accessed: 10- May- 2022].

[14] A. Chen, J. Ryu, P. Donald, and A. Colevas, "Cancer of the Nasal Cavity and Paranasal Sinuses", 2022.

[15] S. M. Shelke and S. W. Mohod, "Automated Segmentation and Detection of Brain Tumor from MRI", *Ieeexplore.ieee.org*, 2022. [Online]. Available: https://ieeexplore.ieee.org/document/8554807/. [Accessed: 10- May- 2022].

[16] M. Huang et al., "Content-Based Image Retrieval Using Spatial Layout Information in Brain Tumor T1-Weighted Contrast-Enhanced MR Images", *PLoS ONE*, vol. 9, no. 7, p. e102754, 2014. Available: 10.1371/journal.pone.0102754.

[17] J. Cheng et al., "Correction: Enhanced Performance of Brain Tumor Classification via Tumor Region Augmentation and Partition", *PLOS ONE*, vol. 10, no. 12, p. e0144479, 2015. Available: 10.1371/journal.pone.0144479.

[18] Z. Li et al., "Low-Grade Glioma Segmentation Based on CNN with Fully Connected CRF", *Journal of Healthcare Engineering*, vol. 2017, pp. 1-12, 2017. Available: 10.1155/2017/9283480 [Accessed 10 May 2022].

[19] N. Arunkumar, M. Mohammed, S. Mostafa, D. Ibrahim, J. Rodrigues, and V. Albuquerque, "Fully automatic model-based segmentation and classification approach for MRI brain tumor using artificial neural networks", *Concurrency and Computation: Practice and Experience*, vol. 32, no. 1, 2018. Available: 10.1002/cpe.4962 [Accessed 10 May 2022].

[20] W. Chen, B. Liu, S. Peng, J. Sun, and X. Qiao, "S3D-UNet: Separable 3D U-Net for Brain Tumor Segmentation", *Brainlesion: Glioma, Multiple Sclerosis, Stroke and Traumatic Brain Injuries*, pp. 358-368, 2019. Available: 10.1007/978-3-030-11726-9_32 [Accessed 10 May 2022].

[21] H. H. Sultan, N. M. Salem, and W. Al-Atabany, "Multi-Classification of Brain Tumor Images Using Deep Neural Network," in *IEEE Access*, vol. 7, pp. 69215-69225, 2019, doi: 10.1109/ACCESS.2019.2919122.

[22] A. Alqudah, "Brain Tumor Classification Using Deep Learning Technique - A Comparison between Cropped, Uncropped, and Segmented Lesion Images with Different Sizes", *International Journal of Advanced Trends in Computer Science and Engineering*, vol. 8, no. 6, pp. 3684-3691, 2019. Available: 10.30534/ijatcse/2019/155862019 [Accessed 10 May 2022].

[23] M. Sharif, J. Li, M. Khan, and M. Saleem, "Active deep neural network features selection for segmentation and recognition of brain tumors using MRI images", *Pattern Recognition Letters*, vol. 129, pp. 181-189, 2020. Available: 10.1016/j.patrec.2019.11.019 [Accessed 10 May 2022].

[24] S. Abdelaziz Ismael, A. Mohammed and H. Hefny, "An enhanced deep learning approach for brain cancer MRI images classification using residual networks", *Artificial Intelligence in Medicine*, vol. 102, p. 101779, 2020. Available: 10.1016/j.artmed.2019.101779 [Accessed 10 May 2022].

[25] M. Badža and M. Barjaktarović, "Classification of Brain Tumors from MRI Images Using a Convolutional Neural Network", *Applied Sciences*, vol. 10, no. 6, p. 1999, 2020. Available: 10.3390/app10061999 [Accessed 10 May 2022].

[26] M. Ali, S. Gilani, A. Waris, K. Zafar, and M. Jamil, "Brain Tumour Image Segmentation Using Deep Networks", *IEEE Access*, vol. 8, pp. 153589-153598, 2020. Available: 10.1109/access.2020.3018160 [Accessed 10 May 2022].

[27] W. Wu et al., "An Intelligent Diagnosis Method of Brain MRI Tumor Segmentation Using Deep Convolutional Neural Network and SVM Algorithm", *Computational and Mathematical Methods in Medicine*, vol. 2020, pp. 1-10, 2020. Available: 10.1155/2020/6789306 [Accessed 10 May 2022].

[28] M. Rehman, S. Cho, J. Kim, and K. Chong, "BU-Net: Brain Tumor Segmentation Using Modified U-Net Architecture", *Electronics*, vol. 9, no. 12, p. 2203, 2020. Available: 10.3390/electronics9122203 [Accessed 10 May 2022].

[29] F. Díaz-Pernas, M. Martínez-Zarzuela, M. Antón-Rodríguez, and D. González-Ortega, "A Deep Learning Approach for Brain Tumor Classification and Segmentation Using a Multiscale Convolutional Neural Network", *Healthcare*, vol. 9, no. 2, p. 153, 2021. Available: 10.3390/healthcare9020153 [Accessed 10 May 2022].

[30] M. Aghalari, A. Aghagolzadeh and M. Ezoji, "Brain tumor image segmentation via asymmetric/symmetric UNet based on two-pathway-residual blocks", *Biomedical Signal Processing and Control*, vol. 69, p. 102841, 2021. Available: 10.1016/j.bspc.2021.102841 [Accessed 10 May 2022].

[31] B. Elshaikh, M. Garelnabi, H. Omer, A. Sulieman, B. Habeeballa and R. Tabeidi, "Recognition of brain tumors in MRI images using texture analysis", *Saudi Journal of Biological Sciences*, vol. 28, no. 4, pp. 2381-2387, 2021. Available: 10.1016/j.sjbs.2021.01.035 [Accessed 10 May 2022].

[32] E. Irmak, "Multi-Classification of Brain Tumor MRI Images Using Deep Convolutional Neural Network with Fully Optimized Framework", *Iranian Journal of Science and Technology, Transactions of Electrical Engineering*, vol. 45, no. 3, pp. 1015-1036, 2021. Available: 10.1007/s40998-021-00426-9 [Accessed 10 May 2022].

[33] D. Nayak, N. Padhy, P. Mallick, M. Zymbler and S. Kumar, "Brain Tumor Classification Using Dense Efficient-Net", *Axioms*, vol. 11, no. 1, p. 34, 2022. Available: 10.3390/axioms11010034 [Accessed 10 May 2022].

[34] C. Srinivas et al., "Deep Transfer Learning Approaches in Performance Analysis of Brain Tumor Classification Using MRI Images", *Journal of Healthcare Engineering*, vol. 2022, pp. 1-17, 2022. Available: 10.1155/2022/3264367 [Accessed 10 May 2022].

[35] "Magnetic resonance imaging - Wikipedia", *En.wikipedia.org*, 2022. [Online]. Available: https://en.wikipedia.org/wiki/Magnetic_resonance_imaging#:~:text=Magnetic%20resonance%20imaging%20(MRI)%20is,the%20organs%20in%20the%20body. [Accessed: 10- May- 2022]..

[36]"MRI Basics", *Case.edu*, 2022. [Online]. Available: https://case.edu/med/neurology/NR/MRI%20Basics.htm#:~:text=The%20most%20common%20MRI%20sequences,longer%20TE%20and%20TR%20times. [Accessed: 10- May- 2022].

[37]"brain tumor dataset", *figshare*, 2022. [Online]. Available: https://figshare.com/articles/dataset/brain_tumor_dataset/1512427. [Accessed: 10- May- 2022].

[38] “Brain Tumor MRI Dataset" , *Kaggle.com*, 2022. [Online]. Available: https://www.kaggle.com/datasets/masoudnickparvar/brain-tumor-mri-dataset. [Accessed: 10- May- 2022].

[39] “Complete Architectural Details of all EfficientNet Models”, Medium, 2022. [Online]. Available: https://towardsdatascience.com/complete-architectural-details-of-all-efficientnet-models-5fd5b736142. [Accessed: 10- May- 2022].

[40] O. Ronneberger, P. Fischer, and T. Brox. U-net: Convolutional networks for biomedical image segmentation. In International Conference on Medical Image Computing and Computer-Assisted Intervention, 2015. Available: https://doi.org/10.48550/arXiv.1505.04597.

[41] M. Zhou et al., "Radiomics in Brain Tumor: Image Assessment, Quantitative Feature Descriptors, and Machine-Learning Approaches", American Journal of Neuroradiology, vol. 39, no. 2, pp. 208-216, 2017. Available: 10.3174/ajnr.a5391.

[42] "tkinter — Python interface to Tcl/Tk — Python 3.10.4 documentation", *Docs.python.org*, 2022. [Online]. Available: https://docs.python.org/3/library/tkinter.html. [Accessed: 10- May- 2022].

[43] "mAP (mean Average Precision) might confuse you!", *Medium*, 2022. [Online]. Available: https://towardsdatascience.com/map-mean-average-precision-might-confuse-you-5956f1bfa9e2. [Accessed: 10- May- 2022].

[44] “Mzoughi et al., "Deep Multi-Scale 3D Convolutional Neural Network (CNN) for MRI Gliomas Brain Tumor Classification", *Journal of Digital Imaging*, vol. 33, no. 4, pp. 903-915, 2020. Available: 10.1007/s10278-020-00347-9 [Accessed 10 May 2022].

[45] R. Hashemzehi, S. Mahdavi, M. Kheirabadi and S. Kamel, "Detection of brain tumors from MRI images base on deep learning using hybrid model CNN and NADE", *Biocybernetics and Biomedical Engineering*, vol. 40, no. 3, pp. 1225-1232, 2020. Available: 10.1016/j.bbe.2020.06.001 [Accessed 10 May 2022].

[46] Sajja, V.R. Classification of Brain tumors using Fuzzy C-means and VGG16. Turk. J. Comput. Math. Educ. (TURCOMAT), vol. 12, pp. 2103–2113, 2021, Available: https://doi.org/10.17762/turcomat.v12i9.3680

[47] "Google Colab", *Research.google.com*, 2022. https://research.google.com/colaboratory/faq.html. [Accessed: 10- May- 2022].

[48] "Is the Dice coefficient the same as accuracy?", *Cross Validated*, 2022. [Online]. Available: https://stats.stackexchange.com/questions/195006/is-the-dice-coefficient-the-same-as-accuracy#:~:text=The%20Dice%20score%20is%20often,how%20similar%20the%20objects%20are. [Accessed: 10- May- 2022].

[49] "Structural similarity - Wikipedia", *En.wikipedia.org*, 2022. [Online]. Available: https://en.wikipedia.org/wiki/Structural_similarity#:~:text=The%20structural%20similarity%20index%20measure,the%20similarity%20between%20two%20images. [Accessed: 10- May- 2022].

[50] "Mean squared error - Wikipedia", *En.wikipedia.org*, 2022. [Online]. Available: https://en.wikipedia.org/wiki/Mean_squared_error. [Accessed: 10- May- 2022].

[51] "Jaccard Index / Similarity Coefficient", *Statistics How To*, 2022. [Online]. Available: https://www.statisticshowto.com/jaccardindex/#:~:text=The%20Jaccard%20similarity%20index%20(sometimes,more%20similar%20the%20two%20populations. [Accessed: 10- May- 2022].

[52] "MICCAI BraTS 2018: Data | Section for Biomedical Image Analysis (SBIA) | Perelman School of Medicine at the University of Pennsylvania", *Med.upenn.edu*, 2022. [Online]. Available: https://www.med.upenn.edu/sbia/brats2018/data.html. [Accessed: 10- May- 2022].

[53] Z. Zhou, M. Siddiquee, N. Tajbakhsh and J. Liang, "UNet++: Redesigning Skip Connections to Exploit Multiscale Features in Image Segmentation", *IEEE Transactions on Medical Imaging*, vol. 39, no. 6, pp. 1856-1867, 2020. Available: 10.1109/tmi.2019.2959609 [Accessed 10 May 2022].